

LOFT: Low-Rank Orthogonal Fine-Tuning via Task-Aware Support Selection

Lanxin Zhao* Bamdev Mishra† Pratik Jawanpuria‡ Lequan Lin* Dai Shi§
 Junbin Gao* Andi Han*

Abstract

Orthogonal parameter-efficient fine-tuning (PEFT) adapts pretrained weights through structure-preserving multiplicative transformations, but existing methods often conflate two distinct design choices: the subspace in which adaptation occurs and the transformation applied within that subspace. This paper introduces LOFT, a low-rank orthogonal fine-tuning framework that explicitly separates these two components. By viewing orthogonal adaptation as a multiplicative subspace rotation, LOFT provides a unified formulation that recovers representative orthogonal PEFT methods, including coordinate-, butterfly-, Householder-, and principal-subspace-based variants. More importantly, this perspective exposes support selection as a central design axis rather than a byproduct of a particular parameterization. We develop a first-order analysis showing that useful adaptation supports should be informed by the downstream training signal, motivating practical task-aware support selection strategies. Across language understanding, visual transfer, mathematical reasoning, and multilingual out-of-distribution adaptation, LOFT recovers principal-subspace orthogonal adaptation while gradient-informed supports improve the efficiency–performance trade-off under matched parameter, memory, and compute budgets. These results suggest that principled support selection is an important direction for improving orthogonal PEFT.

1 Introduction

Foundation models are increasingly being adapted to a wide range of downstream tasks, domains, and deployment environments. As model scale grows, however, maintaining a separately fully fine-tuned model for each task becomes increasingly costly in optimization, storage, and inference, especially in multi-task or resource-constrained settings (Hu et al., 2021; Han et al., 2024). Parameter-efficient fine-tuning (PEFT) addresses this problem by keeping the pretrained backbone fixed and learning only a small task-specific modification.

Within reparameterization-based PEFT, two complementary paradigms have emerged. One line is additive and low-rank: LoRA (Hu et al., 2021) models downstream adaptation as a compact low-dimensional perturbation, and later methods such as PiSSA (Meng et al., 2024) and DoRA (Liu et al., 2024a) refine how that perturbation is initialized or decomposed. A second line, which is the

*The University of Sydney, Australia. lzha6608@uni.sydney.edu.au, lequan.lin@sydney.edu.au, junbin.gao@sydney.edu.au, andi.han@sydney.edu.au

†Microsoft India. bamdevm@microsoft.com

‡Indian Institute of Technology Bombay, India. pratik.jawanpuria@iitb.ac.in

§University of Cambridge, UK. ds2213@cam.ac.uk

focus of this paper, is multiplicative and geometric: orthogonal fine-tuning adapts frozen weights through multiplicative transforms that aim to preserve pretrained structure while still allowing task-specific change (Qiu et al., 2023; Liu et al., 2024b; Ma et al., 2024; Yuan et al., 2024; Wu et al., 2026). The appeal of the orthogonal view is geometric: unlike additive low-rank updates, a multiplicative orthogonal transform exactly preserves the structure of the pretrained weight, so adaptation is constrained to act as a change of basis on top of a fixed pretrained geometry. Although these lines are often presented separately, both rely on the same underlying picture: effective adaptation is concentrated on a low-dimensional subspace, which we call the *adaptation support*, and methods differ primarily in what transformation is allowed to act on that support.

A characteristic feature of existing orthogonal PEFT methods is that the support and the transform are tightly coupled inside a single parameterization. Block-diagonal transforms (Qiu et al., 2023), butterfly factorizations (Liu et al., 2024b), Givens rotations (Ma et al., 2024), Householder reflections (Yuan et al., 2024), and principal-subspace restrictions (Wu et al., 2026) are introduced as different ways to parameterize the orthogonal action, but each of them couples the effective support with a particular transform parameterization. As a result, the support is treated as a built-in property of the method rather than as a design variable that one can compare across methods. This coupling makes it hard to tell whether a reported improvement comes from a better orthogonal parameterization, a different effective support, or a combination of the two.

To make this distinction explicit, we introduce **Low-rank orthogonal Fine-Tuning (LOFT)**, a multiplicative subspace-rotation framework that separates the adaptation support P_r from the in-subspace transform $T_r \in \mathbb{R}^{r \times r}$, with the update as $W^+x = W_0(I_{d_{\text{in}}} + P_r^\top(T_r - I_r)P_r)x$, so that a row orthonormal matrix $P_r \in \mathbb{R}^{r \times d_{\text{in}}}$ determines *where* adaptation acts and T_r determines *how* the selected subspace is transformed. Under this view, several existing orthogonal PEFT methods can be expressed as specific instances of the same primitive by varying the support basis, factor width, factor depth, and in-subspace transform class, rather than appearing as fundamentally distinct mechanisms.

This reformulation poses a natural question: *which support is most useful for downstream adaptation, and is there a principled, task-aware way to construct P_r ?* Existing orthogonal PEFT methods choose the support in a task-agnostic way—as a fixed coordinate or butterfly partition of the input space (Qiu et al., 2023; Liu et al., 2024b; Ma et al., 2024), or as the principal right singular subspace of the pretrained weight (Wu et al., 2026). Such choices use no information about the downstream task, and there is no a priori reason for the resulting P_r to align with directions along which the downstream loss is most easily reduced, particularly when the downstream task departs from the pretraining distribution. Motivated by a first-order analysis of the orthogonal-adaptation training dynamics, we propose a complementary, task-aware way to construct P_r from downstream gradient signals computed at the pretrained weight.

Our contributions are summarized as follows:

- **Framework.** We introduce LOFT, an orthogonal PEFT framework that decomposes the adaptation into a support P_r and an in-subspace transform T_r . When T_r is orthogonal, the framework preserves the pretrained structure exactly. We show existing representative orthogonal PEFT methods can be expressed as specific instances of this primitive.
- **Gradient-informed support selection.** Within the framework, we give a first-order analysis showing that the local training signal of a right-subspace orthogonal update is governed by $\text{skew}(W_0^\top G)$, where G is the gradient at W_0 , and use this analysis to motivate two practical

gradient-informed supports, GRADSVD and SKEWGRAD, as new options for P_r alongside the principal-weight support used by spectral orthogonal PEFT.

- **Controlled empirical study.** We use the framework to compare principal and gradient-informed supports under matched parameter, memory, and transform budgets across language understanding, visual transfer, and mathematical reasoning. The experiments indicate that the support is a meaningful design axis: principal-support LOFT recovers the closest spectral baseline, and gradient-informed supports can improve the efficiency–performance trade-off in our settings.

2 Methodology

2.1 Preliminary on Orthogonal Fine-tuning

We consider orthogonal parameter-efficient adaptation of a pretrained linear weight matrix $W_0 \in \mathbb{R}^{d_{\text{out}} \times d_{\text{in}}}$, and let $L(W)$ denote the downstream objective evaluated at weight W . We write $O(d)$ for the orthogonal group and $\text{Skew}(d) := \{S \in \mathbb{R}^{d \times d} : S^\top = -S\}$ for the space of skew-symmetric matrices. We also define $\text{skew}(A) = (A - A^\top)/2$. For a row-orthonormal support $P_r \in \mathbb{R}^{r \times d_{\text{in}}}$ with $P_r P_r^\top = I_r$, the matrix $\Pi_r := P_r^\top P_r$ is the orthogonal projection onto the selected r -dimensional right subspace. In Appendix A, we also include additional related works.

Orthogonal Fine-tuning. Orthogonal fine-tuning (Qiu et al., 2023) proposes to adapt pretrained weight W_0 by an orthogonal transformation, i.e.,

$$W^+ = W_0 U, \quad W_0 \in \mathbb{R}^{d_{\text{out}} \times d_{\text{in}}}, U \in O(d_{\text{in}}),$$

which preserves the pairwise neuron similarity of the pretrained model, i.e., $W^+ W^{+\top} = W_0 W_0^\top$. By contrast, the standard additive adaptation $W^+ = W_0 + \Delta W$ places no structural constraint on ΔW , and thus offers no guarantee on the geometry of the resulting weight matrix. The seminal work, LoRA (Hu et al., 2021) restricts ΔW to have rank at most r via the factorization $\Delta W = AB$, achieving parameter efficiency but still lacking geometric control. LOFT builds on the geometry-preserving view of orthogonal fine-tuning, while confining the transformation to an explicit low-dimensional support subspace.

2.2 LOFT: a Unified Framework for Orthogonal PEFT

We formulate parameter-efficient orthogonal adaptation as a multiplicative transform acting on a selected low-dimensional input subspace. Let $P \in O(d_{\text{in}})$, and denote P_r as the first r rows of P , $P_r \in \mathbb{R}^{r \times d_{\text{in}}}$, which forms row-orthonormal support basis with $P_r P_r^\top = I_r$, and let $T_r \in \mathbb{R}^{r \times r}$ be the learnable transform within this support. We parameterize the update as

$$S(P_r, T_r) := P^\top \begin{bmatrix} T_r & 0 \\ 0 & I_{d_{\text{in}}-r} \end{bmatrix} P = I_{d_{\text{in}}} + P_r^\top (T_r - I_r) P_r, \quad W^+ = W S(P_r, T_r).$$

Equivalently, $W^+ = W(I_{d_{\text{in}}} - P_r^\top P_r) + W P_r^\top T_r P_r$, so the selected subspace is transformed by T_r , while its orthogonal complement is left unchanged. This cleanly separates two design choices: P_r determines *where* adaptation acts, and T_r determines *how* the selected subspace is transformed. Notably, when $T_r \in O(r)$, $S(P_r, T_r) \in O(d_{\text{in}})$.

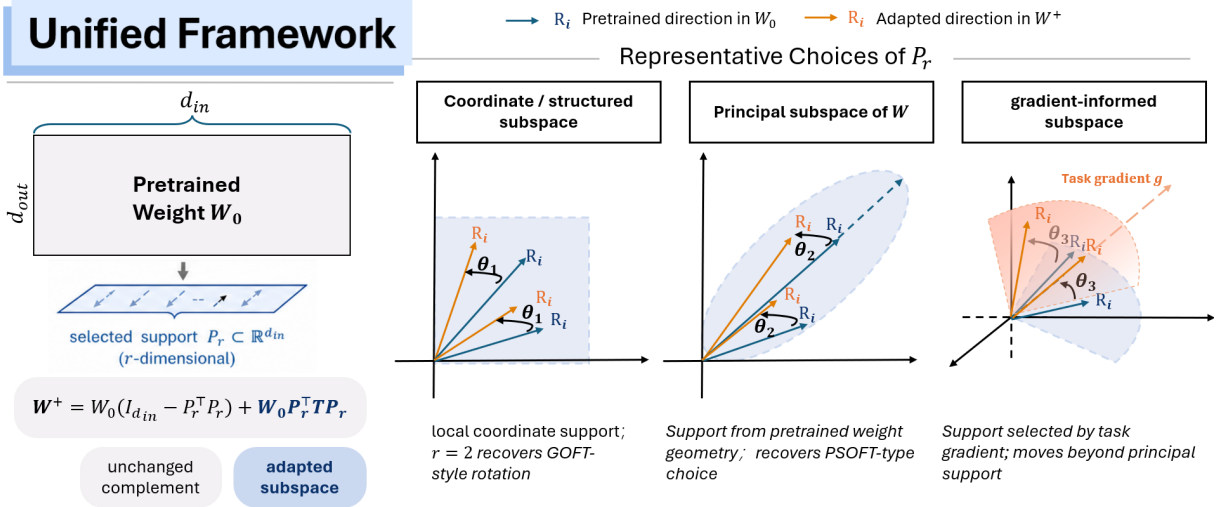


Figure 1: **LOFT as right-subspace adaptation.** Left: LOFT updates the pretrained weight W_0 by applying an in-subspace transform T_r only on the selected right support P_r , while leaving the orthogonal complement unchanged. Right: different choices of P_r , including coordinate, principal, random, and task-informed supports, instantiate different orthogonal PEFT regimes within the same right-multiplicative form $W^+ = W_0(I + P_r^T(T_r - I_r)P_r)$.

Remark 1 (Connection to Group Theory). *For a fixed support P_r , the map $S(P_r, \cdot)$ is a Lie group embedding of $O(r)$ into $O(d_{\text{in}})$, whose image is a closed Lie subgroup. Thus, the choice of P_r selects which Lie subgroup the training optimizes over.*

In the following proposition, we show the favorable properties of orthogonal fine-tuning, such as spectral norm and rank, are preserved under LOFT parameterization. This is shown to retain the pretrained model’s learned representations structurally, improve training stability, and mitigate catastrophic forgetting (Qiu et al., 2023; 2025).

Proposition 1 (Geometry Preservation). *If $P_r P_r^T = I_r$ and $T_r \in O(r)$, then $S(P_r, T_r) \in O(d_{\text{in}})$. Therefore, for $W^+ = W S(P_r, T_r)$,*

$$W^+ W^{+\top} = W W^\top, \quad \text{rank}(W^+) = \text{rank}(W), \quad \sigma_i(W^+) = \sigma_i(W) \quad \forall i,$$

where σ_i are singular values, and consequently $\|W^+\|_F = \|W\|_F$ and $\|W^+\|_2 = \|W\|_2$.

More generally, LOFT can compose multiple orthogonal transforms,

$$W^+ = W \prod_{\ell=1}^L S\left(P_{r_\ell}^{(\ell)}, T_{r_\ell}^{(\ell)}\right),$$

which explores the subgroup of $O(d_{\text{in}})$ generated by L products of $O(r_\ell)$, $\ell = 1, \dots, L$. The composition is able to explore a larger subgroup depending on the diversity of supports $P^{(\ell)}$. This exposes multiple design axes: factor depth L , factor width $\{r_\ell\}$, and support selection $\{P_{r_\ell}^{(\ell)}\}$. Figure 1 summarizes the decomposition.

2.3 Recovering Orthogonal PEFT Methods

In this section, we show how the core multiplicative updates of several representative orthogonal fine-tuning methods can be written as special cases of LOFT under different choices of factor depth, factor width, and subspace basis. Table 1 summarizes the design-level correspondences, while Appendix C.1 provides expanded derivations.

Table 1: LOFT design map of representative orthogonal PEFT branches.

Methods	P_r	Width/Depth	Transform	Core mechanism
Full OFT (Qiu et al., 2023)	$I_{d_{\text{in}}}$	$r = d_{\text{in}}, L = 1$	$T_r \in O(d_{\text{in}})$	Full orthogonal fine-tuning, $W^+ = WT_r$.
Block OFT (Qiu et al., 2023)	coordinate blocks	block width b	$T_b \in O(b)$	Disjoint coordinate-block rotations forming a block-diagonal transform.
GOFT (Ma et al., 2024)	coordinate pairs	width 2, depth L	$T_2(\theta)$	Products of 2D coordinate-plane rotations.
BOFT (Liu et al., 2024b)	butterfly blocks	width b , multi-stage	$T_b \in O(b)$	Sparse block rotations composed across butterfly stages.
HRA (Yuan et al., 2024)	learnable u_ℓ^\top	width 1, depth L	$T_1 = -1$	Products of Householder reflections, $I - 2u_\ell u_\ell^\top$.
PSOFT (Wu et al., 2026)	V_r^\top	$r < d_{\text{in}}, L = 1$	$T_r \in O(r)$	Rotation inside the principal right-singular subspace of W_0 .

Several specializations are particularly relevant for subsequent discussions. When $r = 2$ and P_r is formed by two rows of a permutation matrix, LOFT applies a Givens rotation to the selected coordinate plane, thus recovering GOFT (Ma et al., 2024). When $r = 1$, $P_r = u^\top$ with $\|u\|_2 = 1$, and $T_1 = -1$, LOFT gives $S(u^\top, -1) = I - 2uu^\top$. Thus products of Householder reflections (Yuan et al., 2024) correspond to LOFT depth with learnable width-one subspace bases and fixed in-subspace reflections. When P_r is selected to be the top right-singular subspace of W_0 , i.e., $P_r = V_r^\top$, where $W_0 = U_r \Sigma_r V_r^\top + U_\perp \Sigma_\perp V_\perp^\top$, LOFT gives $W^+ = U_\perp \Sigma_\perp V_\perp^\top + U_r \Sigma_r T_r V_r^\top$, which reduces to PSOFT (Wu et al., 2026) up to additional scaling components and relaxation designs.

2.4 Task-Aware Adaptation Support Selection

Despite the empirical success of parameter-efficient orthogonal fine-tuning, the selection of the support subspace has received little attention. Existing works (e.g., PSOFT (Wu et al., 2026)) are mostly task-agnostic, with the support determined by pretrained structure. This offers no guarantee that the chosen subspace aligns with the downstream signal. *In the following, we provide a principled way to determine the support based on the initial training signal.*

Specifically, we parameterize the low-dimensional orthogonal transform $T_r = Q(E) \in O(r)$ for $E \in \text{Skew}(r)$, where $Q(\cdot) : \text{Skew}(r) \rightarrow O(r)$ such that $Q(0) = I_r, dQ(tE)/dt|_{t=0} = E$. Examples of such Q include Cayley transform (Qiu et al., 2023; Wu et al., 2026) and matrix exponential. Consider the proposed LOFT update $W^+ = W_0(I + P_r^\top(Q(E) - I_r)P_r)$, where we optimize over $E \in \text{Skew}(r)$ from zero initialization because when $E = 0$, $W^+ = W_0$. The next proposition derives the gradient with respect to E at initialization.

Proposition 2 (Initial Training Gradient). *Let W_0 be the pretrained weight, and let $G = \nabla_W L|_{W=W_0}$ be the gradient of downstream loss at W_0 . We define $\tilde{L}(E_t) := L(W_0(I + P_r^\top(Q(E_t) - I_r)P_r))$. For any $E \in \text{Skew}(r)$, it satisfies that*

$$\left. \frac{d}{dt} L\left(W_0\left(I + P_r^\top(Q(tE) - I_r)P_r\right)\right) \right|_{t=0} = \left\langle P_r \text{skew}(W_0^\top G) P_r^\top, E \right\rangle.$$

Equivalently, on $\text{Skew}(r)$, the projected gradient and its norm satisfy

$$\nabla_{E_t} \tilde{L}|_{E_t=0} = P_r \text{skew}(W_0^\top G) P_r^\top, \quad \|\nabla_{E_t} \tilde{L}|_{E_t=0}\|_F^2 = \|P_r \text{skew}(W_0^\top G) P_r^\top\|_F^2 \leq 2 \sum_{k=1}^{r/2} \mu_k^2.$$

where the nonzero eigenvalues of $\text{skew}(W_0^\top G)$ are $\{\pm i\mu_k\}$ with $\mu_1 \geq \mu_2 \geq \dots \geq 0$. Equality is achieved when P_r spans the invariant subspace of F associated with the largest $\lfloor r/2 \rfloor$ skew-eigenvalue pairs.

Proposition 2 proves that the training signal (measured by gradient norm) is maximized when the support P_r spans the top invariant subspace of $\text{skew}(W_0^\top G)$.¹

Gradient based support selection. Motivated by the first-order analysis, we propose two gradient-based support selection strategies that capture downstream task information.

- SKEWGRAD: choosing P_r to span the top-invariant subspace of $\text{skew}(W_0^\top G)$.
- GRADSVD: choosing P_r to be the top right singular subspace of gradient G .

In our *implementation*, G is estimated once (via a forward and backward pass) from a small calibration set, and the resulting support is fixed during training. In Section 3.5, we show that the one-off computational cost is marginal compared to the principal support. We also highlight that it may further reduce the runtime under optimized implementation, such as gradient reuse.

LOFT is implemented as a fixed-support PEFT adapter on the target linear layers. The adapter applies $x \mapsto S(P_r, T_r)x = x + P_r^\top (T_r - I_r) P_r x$ before the frozen linear projection, which is equivalent to using the merged weight $W^+ = WS(P_r, T_r)$. At inference time, LOFT performs the additive update $\Delta W = W^+ - W = WP_r^\top (T_r - I_r) P_r$. We can show that $\text{rank}(\Delta W) \leq r$. Thus we can view LOFT as multiplicative from its parameterization but low-rank in its induced additive update.

Remark 2 (Optimality under Linearization). *Existing works (Malladi et al., 2023; Jang et al., 2024) have shown that fine-tuning often operates in a near-linear regime: the model remains close to pretrained initialization and is well-approximated by its first-order expansion, the so-called lazy-training or NTK regime (Jacot et al., 2018). Under gradient flow in this regime, the loss evolves as, $L(W^+) \approx L(W) - t \|\nabla_{E_t} \tilde{L}|_{E_t=0}\|_F^2$. So the support that maximizes the initial gradient norm remains approximately optimal throughout training. In contrast, choosing P_r as the top subspace of W_0 (as in PSOFT (Wu et al., 2026)) maximizes pretrained-weight energy $\|W_0 P_r^\top\|_F^2$, which is sub-optimal unless the downstream gradient G aligns with the dominant right-singular directions of W_0 . In practice, this alignment is not guaranteed.*

Remark 3 (Additional Support Choices). *We also highlight additional support choices within the LOFT framework. Rather than a static support, one may consider a dynamic support that evolves over the course of training. In its simplest form, a dynamic random support corresponds to randomized submanifold gradient descent on the orthogonal manifold (Han et al., 2025), which enjoys a global convergence guarantee and, in principle, recovers the full orthogonal fine-tuning. Alternatively, one can adopt a dynamic gradient-informed support by periodically updating the support using gradient information, in a similar spirit to GaLore (Zhao et al., 2024).*

¹We remark that a different parameterization of the low-dimensional orthogonal transform may induce a different support. Nevertheless, the same principle can be applied to derive a gradient-informed support selection criterion.

3 Experiments

Our experiments evaluate the support-selection view of orthogonal PEFT across encoder-only language understanding, mathematical reasoning and visual transfer, organized around the questions: **(1)** Does LOFT recover the principal-subspace orthogonal regime represented by PSOFT as a special case? **(2)** Do task-calibrated supports improve over principal-weight supports under matched parameter and transform budgets? Throughout, we report trainable parameters, peak memory, and task performance. The central empirical observation is that LOFT’s gains stem from selecting a task-aligned support, not merely from a new orthogonal parameterization.

Notation. For LOFT, P_r denotes the adaptation support and T_r the in-subspace transform. We write $P_r = P_{\text{prin}}$ for the principal-weight support from the top right singular subspace of W_0 , $P_r = P_{\text{grad}}$ for GradSVD support from the top right singular subspace of the downstream gradient G , and $P_r = P_{\text{skew}}$ for SkewGrad support from the top invariant subspace of $\text{skew}(W_0^\top G)$. In result tables, LOFT_r^P denotes a LOFT adapter with rank r and support P . Main tables list only the support P_r . Full P_r/T_r ablations are reported for GLUE and VTAB in Appendix G.

Baselines. Across benchmarks, we compare LOFT with representative reparameterization-based PEFT methods. The low-rank family includes LoRA, PiSSA, DoRA, and LoRA-XS (Hu et al., 2021; Meng et al., 2024; Liu et al., 2024a; Bałazy et al., 2024). The orthogonal family includes GOFTv2/qGOFTv2, BOFT, OFTv2, and PSOFT (Ma et al., 2024; Liu et al., 2024b; Qiu et al., 2025; Wu et al., 2026). We cite the baseline families here and refer to them below as the baseline suite; benchmark-specific protocol differences and additional ablations are described in the corresponding appendix sections.

The code is available at <https://github.com/Kris-camp/loft>.

3.1 GLUE on DeBERTaV3-base

Experimental setting. We begin with a controlled encoder-only benchmark on six GLUE tasks CoLA, STS-B, RTE, MRPC, SST-2, and QNLI, using DeBERTaV3-base (He et al., 2021). We follow the same hold-out validation protocol as PSOFT (Wu et al., 2026): the original validation split is partitioned into validation/test subsets with a fixed seed, model selection is performed on the new validation split, and the reported score is the held-out test score of the best validation checkpoint. Results are averaged over five random seeds. Following GLUE convention (Wang et al., 2018), we report Matthews correlation on CoLA, Pearson correlation on STS-B, and accuracy on the remaining tasks.

Table 2: GLUE results on DeBERTaV3-base. Reported values are averaged over five random seeds, and Avg. is highlighted. Mem.(GB) reports peak GPU memory on a single NVIDIA V100 64GB GPU. Full experimental settings are provided in Appendix E.1.

Method	#Params	Mem.(GB)	CoLA	STS-B	RTE	MRPC	SST-2	QNLI	Avg.
FFT	184M	5.9	67.56	91.46	82.88	90.69	94.13	93.37	86.68
GOFTv2	0.08M	18.5	65.45			OOM			N/A
qGOFTv2	0.33M	18.5	68.03			OOM			N/A
BOFT $^b_{m=2}$	1.41M	6.3	68.85	91.09	83.60	88.40	95.28	93.78	86.83
OTv2 $^b_{b=32}$	1.29M	4.5	66.79	91.22	84.03	89.61	93.72	92.64	86.34
LoRA $_{r=8}$	1.33M	4.5	67.98	91.60	84.87	90.20	95.28	93.89	87.30
PiSSA $_{r=8}$	1.33M	4.5	66.50	91.40	83.77	89.90	93.17	92.72	86.24
DoRA $_{r=8}$	1.41M	5.8	67.06	91.60	87.19	90.49	95.23	94.09	87.61
LoRA-XS $_{r=136}$	1.33M	4.2	64.67	91.48	84.17	91.27	93.85	93.14	86.43
PSOFT $_{r=46}$	0.08M	4.1	70.42	91.56	86.74	90.49	95.55	93.47	88.04
LOFT $^P_{r=46}$	0.07M	4.1	70.52	91.37	86.19	90.90	95.73	93.63	88.06
LOFT $^P_{r=46}$	0.07M	4.1	70.63	91.32	87.05	91.67	95.28	94.39	88.39
LOFT $^P_{r=46}$	0.07M	4.1	72.03	91.75	86.83	92.36	95.42	93.97	88.73

In the main text, we report the default orthogonal LOFT transform $T_r = T_{\text{orth}}$ and focus on $P_r = P_{\text{prin}}$ and the proposed $P_r = P_{\text{grad}}$, $P_r = P_{\text{skew}}$. All LOFT results are averaged across five random seeds and the results from the baselines are extracted from (Wu et al., 2026). We report additional LOFT variants in Appendix G.

Main results. From Table 2, LOFT recovers the principal-subspace orthogonal regime with $P_r = P_{\text{prin}}$, where it matches PSOFT with a comparable average score (88.06 vs. 88.04), slightly fewer trainable parameters (0.07M vs. 0.08M), and the same 4.1GB peak memory. The main improvement comes from support selection. Replacing the principal support with the proposed SkewGrad support improves the six-task average to 88.73, without increasing trainable parameters or peak memory. Compared with standard low-rank baselines such as LoRA and DoRA, $\text{LOFT}_{r=46}^{P_{\text{skew}}}$ uses about $20\times$ fewer trainable parameters while achieving a higher average score. This supports the view that P_r is a meaningful design axis: under the same rank, transform class, parameter count, and peak-memory footprint, replacing the pretrained-weight principal support with a loss-informed support improves the efficiency–performance trade-off.

3.2 Mathematical Question Answering on MetaMathQA-40K

Experiment Settings. We consider a matched low-budget setting where all main methods use approximately 0.5M trainable parameters, and report the finalized evaluation result under the tuned learning rate and a shared evaluation pipeline. Implementation details, learning rates, and evaluation scripts are deferred to Appendix E.4.

Main Results. Table 3 shows that the support-selection effect observed on GLUE also transfers to decoder-side mathematical reasoning. Principal-support LOFT remains close to PSOFT, while the task-aware supports improve performance under the same rank and parameter count. GradSVD achieves the best GSM8K score, and SkewGrad achieves the best MATH score, suggesting that downstream optimization signals identify more useful adaptation supports than pretrained principal directions alone.

In terms of memory, all LOFT variants consume a peak GPU memory of 25.68GB, which is the lowest among the compared methods. This corresponds to a 10.4% reduction relative to PSOFT, 48.1% relative to LoRA, 59.4% relative to BOFT, and 79.4% relative to HRA in our implementation. Thus, gradient-informed LOFT improves over principal-support LOFT without increasing memory consumption. Overall, LOFT with gradient-informed support provides a more favorable performance–memory trade-off.

3.3 Visual Transfer on VTAB-1K

Experimental setting. Additionally, we evaluate visual transfer on VTAB-1K (Zhai et al., 2019) by fine-tuning ViT-B/16 (Dosovitskiy et al., 2021) under the standard VTAB-1K transfer protocol. Each task uses 800 labeled training examples for adaptation and 200 validation examples for hyperparameter tuning, and performance is reported as top-1 test accuracy. In the main table, we report the proposed GradSVD and SkewGrad supports under the default orthogonal LOFT transform; principal-support controls and additional support/transform variants are reported in

Table 3: Mathematical reasoning results on GSM8K and MATH under a matched low-budget setting. All methods are run on a single A100-SXM GPU, except HRA, which is run on a single H200-SXM GPU due to OOM on A100-SXM. Mem.(GB) reports peak GPU memory allocated during training, measured with the same instrumentation; details are in Appendix E.4.

Method	#Params	Mem.(GB)	GSM8K	MATH
$\text{BOFT}_{m=1}^{b=2}$	0.786M	63.24	37.33	4.38
$\text{LoRA}_{r=1}$	0.524M	49.5	36.32	4.68
$\text{HRA}_{r=2, \lambda=\infty}$	0.524M	124.92	36.85	5.02
$\text{PSOFT}_{r=128}$	0.536M	28.67	35.94	4.58
Ortho $\text{LOFT}_{r=128}^{\text{prin}}$	0.520M	25.68	34.95	4.98
Ortho $\text{LOFT}_{r=128}^{\text{grad}}$	0.520M	25.68	40.94	5.30
Ortho $\text{LOFT}_{r=128}^{\text{skew}}$	0.520M	25.68	39.65	5.52

Table 4: Experimental results of fine-tuned ViT-B/16 on VTAB-1K. Reported values are top-1 accuracy (%) averaged over five random seeds. Mem.(GB) reports peak GPU memory on a single NVIDIA V100 64GB GPU; full settings are in Appendix E.3.

Method	#Params	Mem.(GB)	Natural							Specialized				Structured						Avg.		
			Cifar100	Caltech101	DTD102	Flower102	Pets	SVHN	Sun397	Camelyon	EuroSAT	Resisc45	Retinopathy	Clevr-Count	Clevr-Dist	DMLab	KITTI-Dist	dSpr-Loc	dSpr-Ori		sNORB-Azi	sNORB-Ele
FFT	85.9M	8.2	70.7	89.3	69.5	99.0	90.4	81.7	54.9	85.4	93.6	83.8	74.5	58.3	51.5	43.2	75.0	73.1	48.7	16.4	30.0	67.8
GOFTv2	0.08M	OOM																				
qGOFTv2	0.33M	OOM																				
BOFT _{m=2} ^{b=8}	1.41M	10.9	70.6	88.2	69.8	99.0	91.4	77.4	55.1	85.1	93.6	82.3	74.9	61.8	50.4	42.9	76.1	73.7	48.8	15.7	30.8	70.9
OFTv2 _{b=32}	1.29M	7.7	68.5	88.9	67.5	98.4	89.5	86.9	53.6	86.0	94.1	84.2	74.6	58.7	56.4	46.7	78.5	81.1	48.1	17.3	32.5	72.1
LoRA _{r=8}	1.33M	9.9	71.4	88.4	70.1	99.0	91.4	76.6	55.7	85.9	94.2	83.3	74.1	72.0	54.3	43.0	76.6	74.8	48.6	16.4	31.8	71.8
PiSSA _{r=8}	1.33M	9.9	70.7	88.7	68.9	99.2	91.0	81.9	53.3	82.6	93.4	83.0	74.0	71.0	60.2	44.0	77.1	81.9	51.8	18.1	33.1	72.3
DoRA _{r=8}	1.41M	17.8	70.7	89.0	69.8	98.9	91.0	81.7	55.5	85.7	94.2	83.5	74.8	67.3	54.2	45.1	77.4	82.0	48.5	16.9	31.5	72.3
LoRA-XS _{r=136}	1.33M	6.6	68.5	89.4	68.4	98.7	90.9	84.5	54.1	84.0	94.3	80.8	73.6	60.0	57.7	45.8	79.6	80.6	48.1	17.4	30.8	71.6
PSOFT _{r=46}	0.08M	6.2	71.9	89.6	70.3	99.1	91.8	86.9	55.9	84.6	94.2	82.4	75.2	71.2	59.9	45.7	79.6	80.9	52.9	20.0	32.9	73.4
LOFT _{r=46} ^{P_{grad}}	0.07M	5.7	69.9	89.6	69.4	99.2	92.0	85.2	55.2	86.4	95.7	82.7	75.3	68.9	59.8	46.2	79.8	79.8	50.2	19.8	33.2	73.3
LOFT _{r=46} ^{P_{skew}}	0.07M	5.7	71.8	90.1	70.2	99.3	92.1	86.2	55.7	86.7	95.0	83.7	75.5	71.2	59.9	46.1	80.1	80.1	52.5	20.0	33.1	73.8

Appendix G. All LOFT results are averaged across five random seeds, and the baseline results are extracted from (Wu et al., 2026).

Main results. Table 4 provides further evidence that support selection is a useful design axis beyond language tasks. SkewGrad gives the strongest VTAB average, improving over PSOFT from 73.4 to 73.8, while using fewer trainable parameters (0.07M vs. 0.08M) and lower peak memory (5.7GB vs. 6.2GB). Compared with standard low-rank baselines such as LoRA and DoRA, LOFT_{r=46}^{P_{skew}} achieves the best average score with roughly an order of magnitude fewer trainable parameters. Since the $r = 46$ principal-support variant in Appendix G does not improve the average, the gain is better explained by support selection than by rank alone.

The main message is that the benefit of task-informed support selection transfers beyond language understanding. Together with the GLUE results, this suggests that SkewGrad captures a general support-selection signal and is not benchmark specific. Although the VTAB gain over PSOFT is modest, it improves the average over all 19 VTAB tasks while using fewer trainable parameters and lower peak memory, supporting the efficiency–performance trade-off of task-informed support selection.

3.4 Training Dynamics under the Matched GLUE Protocol

Table 2 reports the test performance selected by the best validation checkpoint. Here, we ask whether the task-aware support rule only improves this endpoint, or also changes how quickly the model reaches a good solution. This connects the first-order analysis in Proposition 2 to the full-training discussion in Remark 2. Appendix F isolates the initialization-local signal using controlled probe and early-validation diagnostics. At the full-training scale, we find the same support-selection effect: SkewGrad separates from Principal and Random along the training path, reaching lower loss faster and stronger held-out metrics on both CoLA and STS-B under the matched protocol.

For representative GLUE tasks, we report training loss and held-out validation performance at epochs 0, 1, 5, 10, 15, 20. CoLA uses Matthews correlation and STS-B uses Pearson correlation as in Table 2. All variants use the same rank, optimizer, learning-rate schedule, data split, and orthogonal LOFT transform. Only the support P_r is changed: Random, Principal, or SkewGrad. Thus, the

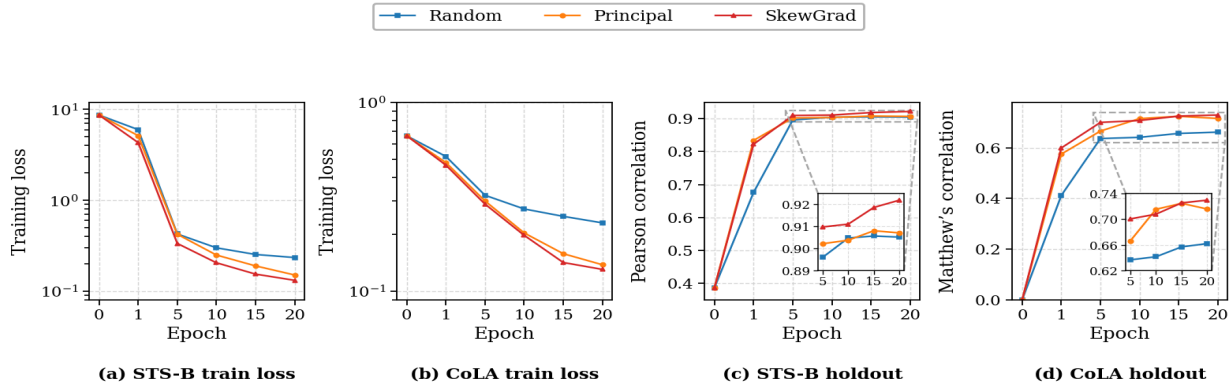


Figure 2: Training dynamics under the matched GLUE protocol. We compare Random, Principal, and SkewGrad supports at epochs 0, 1, 5, 10, 15, 20. Panels (a,b) show training loss on STS-B and CoLA; panels (c,d) show held-out Pearson on STS-B and Matthews on CoLA. All settings are matched, including rank, optimizer, schedule, split, and the orthogonal LOFT transform; the only change is the support P_r .

trajectories isolate the effect of where the orthogonal update is allowed to act.

Figure 2 shows the full training trajectories. On CoLA, the support effect appears early and remains visible throughout training. SkewGrad reaches the low-loss regime faster: by epoch 10, its training loss is already below 0.2, whereas Principal only enters this regime around epoch 15 and Random remains above it over the reported horizon. The held-out trajectory shows the same time-to-performance pattern: SkewGrad crosses 0.70 Matthews correlation by epoch 5, while Principal reaches comparable performance later and Random never reaches this level within 20 epochs. Although Principal is competitive at some intermediate points, SkewGrad gives the best final Matthews correlation, reaching 0.7297 at epoch 20.

The STS-B trajectory gives a complementary view using Pearson correlation as the held-out metric. At epoch 1, both Principal and SkewGrad already improve substantially over Random, with held-out Pearson scores of 0.8342 and 0.8225, compared with 0.6762 for Random. After this initial stage, SkewGrad becomes the strongest support from epoch 5 onward, reaching 0.9098 at epoch 5 and 0.9220 at epoch 20. Principal and Random end at 0.9071 and 0.9052, respectively. Notably, Principal attains lower training loss than SkewGrad at later epochs, but does not achieve the same held-out Pearson, suggesting that SkewGrad follows a better-aligned adaptation path rather than merely minimizing training loss faster.

Together, the CoLA and STS-B trajectories in Figure 2 test whether the first-order support-selection signal is only an initialization artifact or continues to shape optimization under the standard training protocol. The observed dynamics support the latter interpretation: task-aware support selection changes the path of adaptation, not only the final checkpoint selected for reporting. On CoLA, SkewGrad moves the model into a high-performing region earlier; on STS-B, it gives the strongest held-out Pearson from epoch 5 onward and the best final trajectory value. This strengthens the main conclusion of Table 2: SkewGrad improves the efficiency–performance trade-off while keeping rank, transform class, parameter count, and memory footprint fixed.

3.5 Additional Experiment Results

First-order support diagnostics. Appendix F bridges the first-order analysis and the full-training trajectories in Section 3.4. Proposition 2 predicts that supports exposing stronger skew-gradient signal should provide better local descent directions, and the appendix tests this prediction directly. It reports two short-horizon diagnostics: a controlled probe where only the LOFT adapter is updated, and an early-validation diagnostic under the standard GLUE pipeline. Across CoLA and STS-B, stronger skew-gradient signal leads to larger probe-loss reductions, and SkewGrad gives the best early-validation behavior in the first 25 updates. A calibration-size study further shows that only a few training mini-batches are enough to construct an effective SkewGrad support. Together, these diagnostics explain why the trajectories in Section 3.4 improve beyond the endpoint: task-aware supports expose better descent directions from the start, and the full-training results show that this early advantage persists over the training horizon.

GLUE on MNLI and QQP. We report MNLI-matched/QQP experiments in the Appendix E.2. This uses the original GLUE development-set protocol rather than the hold-out protocol in Table 2. The results show a similar efficiency–performance pattern: principal-support LOFT recovers the PSOFT regime, SkewGrad improves over the principal orthogonal support, and the free-transform ablation gives the strongest two-task average, all while using far fewer trainable parameters than standard low-rank baselines.

Low-Resource Language Adaptation. Additional low-resource language experiments in Appendix H.1 provide further support for the same conclusion. Across Bactrian-X languages with different base-model BPB levels, gradient-informed support generally improves over the principal weight-based support, with the largest gains appearing on the strongest OOD language, Swahili. This suggests that the benefit of gradient-informed supports is not specific to GLUE or mathematical reasoning, but also extends to multilingual OOD adaptation.

Runtime Comparisons. Appendix I reports single-seed GLUE wall-clock measurements under the same task-specific protocol as Table 2. At matched rank, orthogonal LOFT uses fewer non-classifier trainable parameters than PSOFT (74,520 vs. 81,144) and is consistently faster; principal-support LOFT is 6.5% faster on average, and SkewGrad remains 6.1% faster even with calibration included. Changing the support has little runtime impact: GradSVD and SkewGrad add only 0.2% and 0.4% average runtime relative to principal support. Free-transform LOFT uses more trainable parameters (152,352) but is substantially faster than orthogonal variants, indicating that runtime is driven more by the in-subspace transform computation than by parameter count alone.

Ablation Studies. Appendices G and H.2 report benchmark-specific ablations: GLUE covers support/transform choices plus MRPC/RTE data-fraction and rank sweeps, while VTAB isolates support selection. Across these settings, the appendix results reinforce the same pattern: principal support recovers the PSOFT-like control, while task-informed supports, especially SkewGrad, produce stronger matched-rank variants. The MRPC/RTE sweeps show this effect persists under reduced supervision and across $r \in \{16, 46, 64\}$, and VTAB tests its transfer to vision. Free transforms help on some sentence-pair tasks but are not uniformly superior. Together, the results identify task-aware support selection, rather than rank increase or relaxed orthogonality, as the main driver.

4 Concluding Remarks

We presented LOFT, a parameter-efficient orthogonal fine-tuning framework that decomposes the update rotation into two explicit choices: the adaptation support P_r and the in-subspace transform

T_r . This view recovers existing orthogonal PEFT methods and more importantly exposes support selection as an important design problem. Our first-order analysis shows that downstream task signal for orthogonal adaptation is governed by $\text{skew}(W_0^\top G)$, rather than by the principal support of the pretrained weight. This motivates task-aware supports such as GRADSVD and SKEWGRAD. Across language understanding, visual transfer, and mathematical reasoning, LOFT variants with gradient-informed supports improve the efficiency–performance trade-off under matched budgets. Overall, LOFT suggests that future progress in orthogonal PEFT should focus not only on better orthogonal parameterizations, but also on principled selection of the support where adaptation occurs.

Limitations. In this work, we focus on the choice of support rather than the orthogonal transform. We use the default Cayley transform on skew-symmetric matrices to parameterize the orthogonal action. In addition, we show that the preferred gradient-informed support can depend on the task family: SkewGrad performs best in our encoder, visual-transfer, and short-horizon studies, while GradSVD is more stable in some decoder-side and multilingual OOD settings. Gradient-informed supports also require a one-off calibration step for gradient computation, slightly increasing the end-to-end runtime compared with the principal-support variant, as reported in Appendix I.

References

- Aghajanyan, A., Gupta, S., and Zettlemoyer, L. (2021). Intrinsic dimensionality explains the effectiveness of language model fine-tuning. In *Proceedings of the 59th Annual Meeting of the Association for Computational Linguistics and the 11th International Joint Conference on Natural Language Processing*, pages 7319–7328. Association for Computational Linguistics.
- Bałazy, K., Banaei, M., Aberer, K., and Tabor, J. (2024). LoRA-XS: Low-rank adaptation with extremely small number of parameters. *arXiv preprint arXiv:2405.17604*.
- Ben Zaken, E., Goldberg, Y., and Ravfogel, S. (2022). BitFit: Simple parameter-efficient fine-tuning for transformer-based masked language-models. In *Proceedings of the 60th Annual Meeting of the Association for Computational Linguistics (Volume 2: Short Papers)*, pages 1–9. Association for Computational Linguistics.
- Dettmers, T., Pagnoni, A., Holtzman, A., and Zettlemoyer, L. (2023). QLoRA: Efficient finetuning of quantized LLMs. In *Advances in Neural Information Processing Systems*, volume 36.
- Dosovitskiy, A., Beyer, L., Kolesnikov, A., Weissenborn, D., Zhai, X., Unterthiner, T., Dehghani, M., Minderer, M., Heigold, G., Gelly, S., Uszkoreit, J., and Houlsby, N. (2021). An image is worth 16x16 words: Transformers for image recognition at scale. In *International Conference on Learning Representations*.
- Han, A., Poirion, P.-L., and Takeda, A. (2025). Efficient optimization with orthogonality constraint: a randomized riemannian submanifold method. *arXiv preprint arXiv:2505.12378*.
- Han, Z., Gao, C., Liu, J., Zhang, J., and Zhang, S. Q. (2024). Parameter-efficient fine-tuning for large models: A comprehensive survey. *arXiv preprint arXiv:2403.14608*.
- He, P., Gao, J., and Chen, W. (2021). DeBERTaV3: Improving DeBERTa using ELECTRA-style pre-training with gradient-disentangled embedding sharing. *arXiv preprint arXiv:2111.09543*.

- Hu, E. J., Shen, Y., Wallis, P., Allen-Zhu, Z., Li, Y., Wang, S., Wang, L., and Chen, W. (2021). LoRA: Low-rank adaptation of large language models. *arXiv preprint arXiv:2106.09685*.
- Jacot, A., Gabriel, F., and Hongler, C. (2018). Neural tangent kernel: Convergence and generalization in neural networks. *Advances in Neural Information Processing Systems*, 31.
- Jang, U., Lee, J. D., and Ryu, E. K. (2024). Lora training in the ntk regime has no spurious local minima. In *International Conference on Machine Learning*, pages 21306–21328. PMLR.
- Karimi Mahabadi, R., Henderson, J., and Ruder, S. (2021). Compacter: Efficient low-rank hyper-complex adapter layers. In *Advances in Neural Information Processing Systems*, volume 34, pages 1022–1035.
- Kopiczko, D. J., Blankevoort, T., and Asano, Y. M. (2024). VeRA: Vector-based random matrix adaptation. In *International Conference on Learning Representations*.
- Lester, B., Al-Rfou, R., and Constant, N. (2021). The power of scale for parameter-efficient prompt tuning. In *Proceedings of the 2021 Conference on Empirical Methods in Natural Language Processing*, pages 3045–3059. Association for Computational Linguistics.
- Li, C., Farkhoor, H., Liu, R., and Yosinski, J. (2018). Measuring the intrinsic dimension of objective landscapes. In *International Conference on Learning Representations*.
- Li, X. L. and Liang, P. (2021). Prefix-tuning: Optimizing continuous prompts for generation. In *Proceedings of the 59th Annual Meeting of the Association for Computational Linguistics and the 11th International Joint Conference on Natural Language Processing (Volume 1: Long Papers)*, pages 4582–4597. Association for Computational Linguistics.
- Lingam, V. C., Tejaswi, A., Vavre, A., Shetty, A., Gudur, G. K., Ghosh, J., Dimakis, A., Choi, E., Bojchevski, A., and Sanghavi, S. (2024). SVFT: Parameter-efficient fine-tuning with singular vectors. In *Advances in Neural Information Processing Systems*, volume 37.
- Liu, H., Tam, D., Muqeeth, M., Mohta, J., Huang, T., Bansal, M., and Raffel, C. A. (2022). Few-shot parameter-efficient fine-tuning is better and cheaper than in-context learning. In *Advances in Neural Information Processing Systems*, volume 35.
- Liu, S.-Y., Wang, C.-Y., Yin, H., Molchanov, P., Wang, Y.-C. F., Cheng, K.-T., and Chen, M.-H. (2024a). DoRA: Weight-decomposed low-rank adaptation. In *International Conference on Machine Learning*.
- Liu, W., Lin, R., Liu, Z., Rehg, J. M., Paull, L., Xiong, L., Song, L., and Weller, A. (2021). Orthogonal over-parameterized training. In *Proceedings of the IEEE/CVF Conference on Computer Vision and Pattern Recognition*, pages 7251–7260.
- Liu, W., Qiu, Z., Feng, Y., Xiu, Y., Xue, Y., Yu, L., Feng, H., Liu, Z., Heo, J., Peng, S., Wen, Y., Black, M. J., Weller, A., and Schölkopf, B. (2024b). Parameter-efficient orthogonal finetuning via butterfly factorization. In *The Twelfth International Conference on Learning Representations*.
- Ma, X., Chu, X., Yang, Z., Lin, Y., Gao, X., and Zhao, J. (2024). Parameter efficient quasi-orthogonal fine-tuning via givens rotation. In *Proceedings of the 41st International Conference on Machine Learning*, volume 235 of *Proceedings of Machine Learning Research*, pages 33686–33729. PMLR.

- Malladi, S., Wettig, A., Yu, D., Chen, D., and Arora, S. (2023). A kernel-based view of language model fine-tuning. In *International Conference on Machine Learning*, pages 23610–23641. PMLR.
- Meng, F., Wang, Z., and Zhang, M. (2024). PiSSA: Principal singular values and singular vectors adaptation of large language models. *arXiv preprint arXiv:2404.02948*.
- Moreno Arcas, A., Sanchis, A., Civera, J., and Juan, A. (2025). HOFT: Householder orthogonal fine-tuning. *arXiv preprint arXiv:2505.16531*.
- Qiu, Z., Liu, W., Feng, H., Xue, Y., Feng, Y., Liu, Z., Zhang, D., Weller, A., and Schölkopf, B. (2023). Controlling text-to-image diffusion by orthogonal finetuning. *Advances in Neural Information Processing Systems*, 36:79320–79362.
- Qiu, Z., Liu, W., Weller, A., and Schölkopf, B. (2025). Orthogonal Finetuning Made Scalable. *arXiv preprint arXiv:2506.19847*.
- Tastan, N., Laskaridis, S., Takac, M., Nandakumar, K., and Horvath, S. (2026). LoFT: Low-rank adaptation that behaves like full fine-tuning. In *International Conference on Learning Representations*.
- Valipour, M., Rezagholizadeh, M., Kobzyev, I., and Ghodsi, A. (2022). DyLoRA: Parameter efficient tuning of pre-trained models using dynamic search-free low-rank adaptation. *arXiv preprint arXiv:2210.07558*.
- Wang, A., Singh, A., Michael, J., Hill, F., Levy, O., and Bowman, S. R. (2018). GLUE: A multi-task benchmark and analysis platform for natural language understanding. *arXiv preprint arXiv:1804.07461*.
- Wu, F., Hu, J., Min, G., and Wang, S. (2026). Efficient orthogonal fine-tuning with principal subspace adaptation. In *International Conference on Learning Representations*.
- Yuan, S., Liu, H., and Xu, H. (2024). Bridging the gap between low-rank and orthogonal adaptation via Householder reflection adaptation. *Advances in Neural Information Processing Systems*, 37:113484–113518.
- Zhai, X., Puigcerver, J., Kolesnikov, A., Ruysen, P., Riquelme, C., Lucic, M., Djolonga, J., Pinto, A. S., Neumann, M., Dosovitskiy, A., Beyer, L., Bachem, O., Tschannen, M., Michalski, M., Bousquet, O., Gelly, S., and Houlsby, N. (2019). A large-scale study of representation learning with the visual task adaptation benchmark. *arXiv preprint arXiv:1910.04867*.
- Zhang, F. and Pilanci, M. (2024). Spectral adapter: Fine-tuning in spectral space. In *Advances in Neural Information Processing Systems*.
- Zhang, Q., Chen, M., Bukharin, A., He, P., Cheng, Y., Chen, W., and Zhao, T. (2023). AdaLoRA: Adaptive budget allocation for parameter-efficient fine-tuning. In *International Conference on Learning Representations*.
- Zhao, J., Zhang, Z., Chen, B., Wang, Z., Anandkumar, A., and Tian, Y. (2024). GaLore: Memory-efficient llm training by gradient low-rank projection. In *International Conference on Machine Learning*, pages 61121–61143. PMLR.

Appendices Contents

A	Related Work	16
B	Additional Theory and Proofs	17
B.1	Proof of Proposition 1	17
B.2	Why LOFT is Right-Multiplicative Rather than Double-Sided	18
B.3	Proof of Proposition 2	18
B.4	Why PSOFT is Generically Suboptimal	19
C	LOFT Design Space and Recovered Orthogonal PEFT Branches	20
C.1	Recovering Right-Multiplicative Orthogonal PEFT Branches	20
C.2	Additional Remarks on the Free Variant	22
D	Construction of Gradient-Based Supports	22
D.1	Naive gradient support (GradSVD)	22
D.2	Orthogonal and Free LOFT	22
E	Additional Experimental Details	23
E.1	GLUE on DeBERTaV3-base	23
E.2	Additional Follow-up on MNLI and QQP	24
E.3	VTAB-1K on ViT-B/16	26
E.4	Mathematical Question Answering on MetaMathQA-40K	27
F	Full Short-Horizon Support Diagnostics	29
F.1	Does the First-Order Signal Predict Support Quality?	30
G	Full Support and Transform Ablations	33
H	Additional Robustness Analyses	36
H.1	Low-Resource Language OOD Adaptation	36
H.2	SkewGrad on MRPC and RTE	38
I	Additional Efficiency Measurements for Principal, GradSVD, and SkewGrad on GLUE	40

A Related Work

Parameter-efficient fine-tuning (PEFT) methods are commonly grouped into selection-based, prompt-based, adapter-based, and reparameterization-based families (Han et al., 2024). Representative examples include BitFit, prefix/prompt tuning, and compact adapter layers (Ben Zaken et al., 2022; Li and Liang, 2021; Lester et al., 2021; Liu et al., 2022; Karimi Mahabadi et al., 2021). Since LOFT belongs to the reparameterization-based line, we focus on methods that adapt pretrained weights directly and can be merged into the backbone without introducing additional inference-time modules.

Low-rank additive adaptation. The dominant reparameterization paradigm models downstream change as an additive perturbation constrained to a low-dimensional space, consistent with evidence that neural-network adaptation often has low intrinsic dimension (Li et al., 2018; Aghajanyan et al., 2021). LoRA established the basic recipe by freezing the pretrained weight and learning a low-rank update that can be merged at inference time (Hu et al., 2021). Subsequent work refined this view from several directions. PiSSA initializes adaptation from the principal singular components of the pretrained weight (Meng et al., 2024), while DoRA separates magnitude and direction so that the adaptation dynamics more closely match those of full fine-tuning (Liu et al., 2024a). Other variants improve rank allocation, quantized training, parameter sharing, compression, or singular-vector structure within the same low-rank paradigm (Zhang et al., 2023; Valipour et al., 2022; Dettmers et al., 2023; Kopiczko et al., 2024; Bałazy et al., 2024; Lingam et al., 2024; Tasthan et al., 2026). This literature strongly supports low-dimensional adaptation, but mainly studies additive updates rather than geometry-preserving multiplicative transformations.

Orthogonal fine-tuning. A complementary line approaches PEFT from a multiplicative and geometric perspective by constraining adaptation to remain orthogonal. Orthogonal over-parameterized training and OFT introduced this view, with OFT using block-diagonal orthogonal transforms to make optimization tractable (Liu et al., 2021; Qiu et al., 2023). BOFT replaces the block-diagonal construction with butterfly factorization, enabling denser information mixing under a parameter-efficient orthogonal parameterization (Liu et al., 2024b). qGOFT uses Givens rotations and relaxed orthogonality to improve flexibility (Ma et al., 2024), while OFTv2 revisits the same line through an input-centric implementation with a Cayley–Neumann approximation (Qiu et al., 2025). Broader orthogonal PEFT variants also include Householder-based methods such as HOFT and SHOFT (Moreno Arcas et al., 2025). For LOFT, the key message is that orthogonal PEFT has largely optimized how to parameterize the transform, while leaving the choice of adaptation support comparatively under-theorized.

Bridging low-rank and orthogonal adaptation. Recent work makes the relation between low-rank and orthogonal PEFT explicit. HRA constructs adapters as products of learnable Householder reflections and interprets the resulting multiplicative update as adaptive low-rank adaptation, with reflection-plane orthogonality controlling the capacity–regularity trade-off (Yuan et al., 2024). Spectral Adapter and related singular-vector methods shift attention from parameterization to spectral placement, studying how subspace restriction changes effective adaptation capacity (Zhang and Pilanci, 2024; Lingam et al., 2024). LoRA-XS is also related in form, since it freezes SVD-derived outer factors and learns a small inner matrix, but it remains an additive low-rank update rather than a multiplicative subspace transform (Bałazy et al., 2024). PSOFT is the closest direct antecedent to our formulation: it restricts orthogonal adaptation to the principal right-singular subspace of the pretrained weight and adds lightweight relaxation during training (Wu et al., 2026). This makes PSOFT an important spectral instance of subspace-restricted orthogonal adaptation, but its support

is chosen by pretrained-weight energy rather than by downstream loss. LOFT generalizes this regime by treating the support P_r as an explicit design variable. Our first-order analysis selects this support through the loss-coupled signal skew($W_0^\top G$), yielding gradient-informed supports that can be compared directly with principal supports under matched budgets.

B Additional Theory and Proofs

B.1 Proof of Proposition 1

Proof. Let

$$U := S(P_r, T_r) = I_{d_{\text{in}}} + P_r^\top (T_r - I_r) P_r.$$

Extend P_r to a full orthogonal basis

$$P = \begin{bmatrix} P_r \\ P_\perp \end{bmatrix} \in O(d_{\text{in}}).$$

Then

$$U = P^\top \begin{bmatrix} T_r & 0 \\ 0 & I_{d_{\text{in}}-r} \end{bmatrix} P.$$

Since $T_r \in O(r)$, the block-diagonal matrix is orthogonal. Hence $U \in O(d_{\text{in}})$.

Now let $W^+ = WU$. Since U is orthogonal,

$$W^+(W^+)^\top = (WU)(WU)^\top = WU U^\top W^\top = WW^\top.$$

This proves exact row-Gram preservation.

Because U is orthogonal, it is invertible. Therefore,

$$\text{rank}(W^+) = \text{rank}(WU) = \text{rank}(W).$$

Moreover,

$$(W^+)^\top W^+ = (WU)^\top (WU) = U^\top W^\top WU.$$

Thus $(W^+)^\top W^+$ is orthogonally similar to $W^\top W$, so the two matrices have the same eigenvalues. Hence W^+ and W have the same singular values:

$$\sigma_i(W^+) = \sigma_i(W) \quad \forall i.$$

Since the Frobenius norm and spectral norm are determined by the singular values, we also have

$$\|W^+\|_F = \|W\|_F, \quad \|W^+\|_2 = \|W\|_2.$$

This proves all claims in Proposition 1. □

B.2 Why LOFT is Right-Multiplicative Rather than Double-Sided

A natural generalization of orthogonal adaptation is the double-sided update

$$W^+ = QWR, \quad Q \in O(d_{\text{out}}), R \in O(d_{\text{in}}).$$

Although this form preserves singular values, it does not preserve the same row-neuron relational structure as right-multiplicative LOFT.

Remark 4. For right-multiplicative orthogonal LOFT, $W^+ = WU$ with $U \in O(d_{\text{in}})$ implies

$$W^+(W^+)^\top = WW^\top.$$

Hence the row Gram matrix is preserved exactly.

In contrast, for a double-sided update $W^+ = QWR$,

$$W^+(W^+)^\top = QWW^\top Q^\top.$$

Therefore the row Gram matrix is generally rotated rather than preserved entrywise. This is the reason we restrict LOFT to the right-multiplicative setting.

B.3 Proof of Proposition 2

Proof. Let

$$F := \text{skew}(W_0^\top G) = \frac{W_0^\top G - G^\top W_0}{2}.$$

For any perturbation $E \in \text{Skew}(r)$, the local condition on Q gives

$$Q(tE) = I_r + tE + o(t).$$

Therefore,

$$W_0 \left(I_d + P_r^\top (Q(tE) - I_r) P_r \right) = W_0 + tW_0 P_r^\top E P_r + o(t).$$

By the first-order expansion of L at W_0 ,

$$\left. \frac{d}{dt} L \left(W_0 \left(I_d + P_r^\top (Q(tE) - I_r) P_r \right) \right) \right|_{t=0} = \left\langle G, W_0 P_r^\top E P_r \right\rangle_F.$$

Using cyclicity of the trace,

$$\left\langle G, W_0 P_r^\top E P_r \right\rangle_F = \text{tr} \left(G^\top W_0 P_r^\top E P_r \right) = \text{tr} \left(P_r G^\top W_0 P_r^\top E \right).$$

Since $E \in \text{Skew}(r)$, only the skew-symmetric part of $P_r W_0^\top G P_r^\top$ contributes to the inner product. Hence

$$\text{tr} \left(P_r G^\top W_0 P_r^\top E \right) = \left\langle \text{skew}(P_r W_0^\top G P_r^\top), E \right\rangle_F.$$

Because $P_r P_r^\top = I_r$, the skew operator commutes with this orthogonal compression:

$$\text{skew}(P_r W_0^\top G P_r^\top) = P_r \text{skew}(W_0^\top G) P_r^\top = P_r F P_r^\top.$$

Thus

$$\frac{d}{dt}L\left(W_0\left(I_d + P_r^\top(Q(tE) - I_r)P_r\right)\right)\Big|_{t=0} = \left\langle P_r F P_r^\top, E \right\rangle_F.$$

Equivalently, under the Frobenius inner product on $\text{Skew}(r)$,

$$\nabla_S L|_{S=0} = P_r F P_r^\top, \quad \|\nabla_S L|_{S=0}\|_F^2 = \|P_r F P_r^\top\|_F^2.$$

It remains to prove the upper bound. Since $F \in \text{Skew}(d)$, its nonzero eigenvalues occur in conjugate pairs $\{\pm i\mu_k\}$, with $\mu_1 \geq \mu_2 \geq \dots \geq 0$. The singular values of F are therefore the values μ_k , each repeated twice. For any row-orthonormal P_r , the compressed matrix $P_r F P_r^\top$ is also skew-symmetric. Let its nonzero eigenvalues be $\{\pm i\nu_j\}_{j=1}^{\lfloor r/2 \rfloor}$, with $\nu_1 \geq \nu_2 \geq \dots \geq 0$. By the variational characterization of singular values for skew-symmetric compressions,

$$\nu_j \leq \mu_j \quad \text{for } j = 1, \dots, \lfloor r/2 \rfloor.$$

Therefore, for even r ,

$$\|P_r F P_r^\top\|_F^2 = 2 \sum_{j=1}^{r/2} \nu_j^2 \leq 2 \sum_{j=1}^{r/2} \mu_j^2.$$

For odd r , the same argument gives the bound with $r/2$ replaced by $\lfloor r/2 \rfloor$.

Equality is achieved when the rows of P_r span the invariant subspace of F associated with the largest $r/2$ skew-eigenvalue pairs. In that case, the compression $P_r F P_r^\top$ contains exactly those largest skew blocks, so its Frobenius norm attains

$$2 \sum_{j=1}^{r/2} \mu_j^2.$$

This proves Proposition 2. □

B.4 Why PSOFT is Generically Suboptimal

The training-signal analysis above yields a precise condition under which the PSOFT choice $P_r = V_r^\top$ is optimal.

Corollary A.8. Assume r is even; for odd r , replace $r/2$ by $\lfloor r/2 \rfloor$ throughout. Let V_r denote the top- r right singular vectors of W_0 , and set $P_r = V_r^\top$. The resulting first-order signal strength is

$$\|V_r^\top F V_r\|_F^2.$$

This achieves the maximal value

$$2 \sum_{k=1}^{r/2} \mu_k^2$$

if and only if $\text{col}(V_r)$ is a maximizing invariant subspace of F , namely an invariant subspace associated with the largest $r/2$ skew-eigenvalue pairs.

Equivalently, writing $V = [V_r \ V_\perp]$ and

$$V^\top F V = \begin{pmatrix} F_{rr} & F_{r\perp} \\ -F_{r\perp}^\top & F_{\perp\perp} \end{pmatrix},$$

a necessary condition is

$$F_{r\perp} = 0,$$

and maximality further requires that the skew-eigenvalue pairs contained in F_{rr} are the largest ones. Generically, even the invariance condition $F_{r\perp} = 0$ does not hold, so principal-subspace orthogonal adaptation is not generically optimal for maximizing the first-order training signal.

C LOFT Design Space and Recovered Orthogonal PEFT Branches

C.1 Recovering Right-Multiplicative Orthogonal PEFT Branches

We now clarify which existing orthogonal PEFT mechanisms are recovered by the right-multiplicative LOFT formulation

$$W^+ = W \prod_{\ell=1}^L S\left(P_{r_\ell}^{(\ell)}, R_{r_\ell}^{(\ell)}\right), \quad S(P_r, R_r) := I + P_r^\top (R_r - I_r) P_r,$$

where each $P_r \in \mathbb{R}^{r \times d_{\text{in}}}$ satisfies $P_r P_r^\top = I_r$ and each $R_r \in O(r)$. The statements below are made at the level of the core right-side subspace-rotation mechanism rather than every implementation detail of a given method.

Full-space OFT. Setting $L = 1$, $r = d_{\text{in}}$, and $P_r = I_{d_{\text{in}}}$ gives

$$S(I, R) = R, \quad W^+ = WR.$$

Therefore, the original full-space orthogonal fine-tuning update is recovered as the width- d_{in} special case of LOFT.

Block-diagonal OFT. Let $\{1, \dots, d_{\text{in}}\}$ be partitioned into k disjoint coordinate blocks of size b , and let $P_b^{(i)}$ select the coordinates of the i -th block. Then

$$W^+ = W \prod_{i=1}^k S\left(P_b^{(i)}, R_b^{(i)}\right).$$

Because the supports are disjoint, the factors commute and reduce to a block-diagonal orthogonal transform,

$$\prod_{i=1}^k S\left(P_b^{(i)}, R_b^{(i)}\right) = \text{diag}\left(R_b^{(1)}, \dots, R_b^{(k)}\right).$$

Hence block-diagonal OFT is recovered by a single right-multiplicative LOFT layer with disjoint coordinate supports.

GOFT / Givens-style coordinate rotations. Suppose each factor has width 2 and selects a coordinate pair:

$$W^+ = W \prod_{\ell=1}^L S\left(P_2^{(\ell)}, R_2^{(\ell)}\right), \quad R_2^{(\ell)} \in O(2).$$

Each factor is then a Givens rotation acting on a selected coordinate plane. This recovers the core coordinate-pair update mechanism underlying GOFT-style orthogonal fine-tuning.

BOFT. BOFT is obtained by stacking multiple right-multiplicative LOFT layers whose supports are coordinate blocks chosen according to the butterfly permutation pattern. Concretely, with block width b and $L = \lceil \log_2 d_{\text{in}} \rceil$ stages,

$$W^+ = W \prod_{\ell=1}^L \prod_{i=1}^{d_{\text{in}}/b} S\left(P_b^{(\ell,i)}, R_b^{(\ell,i)}\right),$$

where within each stage the supports are disjoint, and across stages the supports are permuted in the butterfly pattern. Thus BOFT is recovered as a multi-layer structured sparse special case of the same right-side primitive.

HRA. HRA is recovered by width-one factors with learnable subspace bases. Let $u_i \in \mathbb{R}^{d_{\text{in}}}$ be a unit vector and set

$$P_1^{(i)} = u_i^\top, \quad R_1^{(i)} = -1.$$

Then

$$S(u_i^\top, -1) = I + u_i(-1 - 1)u_i^\top = I - 2u_iu_i^\top,$$

which is exactly a Householder reflection. Therefore,

$$W^+ = W \prod_{i=1}^r \left(I - 2u_iu_i^\top \right)$$

recovers HRA as a product of right-multiplicative width-one reflections. In this case, the trainable degrees of freedom lie in the learnable subspace bases $\{u_i\}$ rather than in $R_1^{(i)}$.

PSOFT / principal-subspace OFT. Let the singular value decomposition of the pretrained weight be

$$W = U\Sigma V^\top, \quad V = [V_r \ V_\perp], \quad U = [U_r \ U_\perp],$$

and choose

$$P_r = V_r^\top.$$

Then

$$W^+ = W(I + V_r(R_r - I_r)V_r^\top) = WV_\perp V_\perp^\top + WV_r R_r V_r^\top = U_\perp \Sigma_\perp V_\perp^\top + U_r \Sigma_r R_r V_r^\top.$$

Hence the residual right-singular subspace remains unchanged, while the principal right-singular subspace undergoes an orthogonal transform. This recovers the core principal-subspace update underlying PSOFT.

Scope of the recovery claims. The recoveries above should be interpreted as statements about the underlying right-multiplicative subspace-rotation mechanism. In particular, LOFT recovers the structural core of full-space, block-diagonal, coordinate-pair, butterfly, Householder, and principal-subspace orthogonal PEFT branches by varying only the depth, width, and subspace basis of the same primitive update.

C.2 Additional Remarks on the Free Variant

The free variant should be interpreted as replacing the orthogonal subspace transform with a fully unconstrained dense linear map

$$T = S, \quad S \in \mathbb{R}^{r \times r},$$

under the same fixed subspace basis P_r . Accordingly, free LOFT is not a mild relaxation of orthogonality, nor a diagonal α, β -style scaling extension. Instead, it is an identity-initialized dense subspace transform with no internal geometric constraint.

This distinction is useful when interpreting experiments: orthogonal and free LOFT differ only in the transformation class within the same selected subspace. Their comparison therefore isolates the effect of enforcing orthogonality once the subspace support is held fixed.

D Construction of Gradient-Based Supports

D.1 Naive gradient support (GradSVD)

For **LOFT-GradSVD**, we construct the fixed support before inserting the fixed- P_r LOFT module. We first identify all target linear layers. We then freeze the model except for the target-layer weights, enable gradients only on those weights, and run forward and backward passes on 4 calibration mini-batches. The weight gradients are accumulated across these calibration batches, producing a gradient matrix G_ℓ for each target layer ℓ . We then perform singular value decomposition on G_ℓ and use its top- r right singular subspace as the fixed support basis $P_{r,\ell}$.

D.2 Orthogonal and Free LOFT

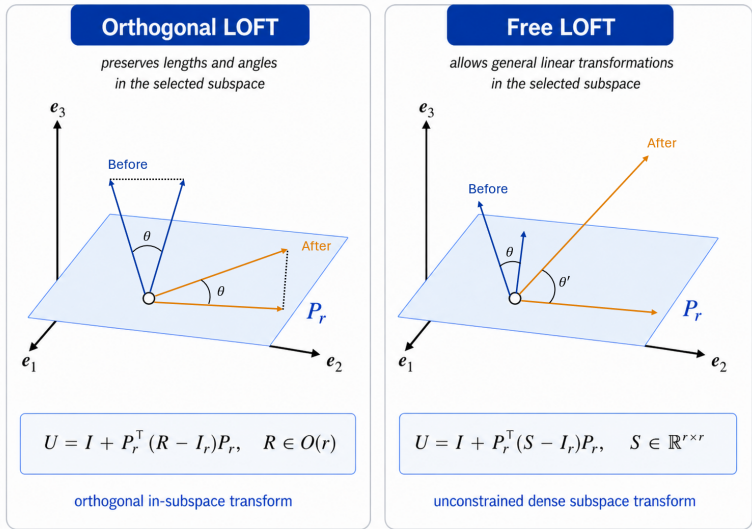


Figure 3: Orthogonal and free LOFT under fixed support P_r .

Once the support basis P_r is fixed, LOFT enables a controlled comparison between two in-subspace transformation classes. In *orthogonal LOFT*, we set $T_r = R_r \in O(r)$, so the ambient transform is orthogonal and Proposition 1 applies directly. In *free LOFT*, we use $T_r = S_r \in \mathbb{R}^{r \times r}$, initialized at I_r

and trained without an internal geometric constraint. Under a fixed support, the difference between orthogonal and free LOFT is entirely attributable to the transformation class acting inside the same selected subspace. Figure 3 visualizes this matched-support comparison: both methods share P_r , but differ in whether the in-subspace transform is constrained to be orthogonal or allowed to be fully free. This distinction is important for the experimental analysis because, once the support is held fixed, comparisons between the two variants isolate the role of the transformation class rather than conflating it with support selection. In later experiments, we therefore use free LOFT only as a controlled ablation of T_r , while keeping the main tables focused on the default orthogonal transform.

E Additional Experimental Details

E.1 GLUE on DeBERTaV3-base

Datasets and metrics. We evaluate encoder-only adaptation on six GLUE tasks: CoLA, STS-B, RTE, MRPC, SST-2, and QNLI. For CoLA we report Matthews correlation, for STS-B we report Pearson correlation, and for RTE, MRPC, SST-2, and QNLI we report accuracy.

Hold-out validation protocol. Following PSOFT, we adopt the same hold-out validation protocol for these six tasks. Specifically, the original validation set of each task is split into new validation and test splits with a fixed random seed. Model selection is performed on the new validation split, and the final reported result is the held-out test score of the checkpoint with the best validation performance. All reported numbers are averaged over five random seeds. Peak memory is measured on a single NVIDIA V100 64GB GPU.

Model and training protocol. We use DeBERTaV3-base as the encoder backbone. Unless otherwise stated, we use AdamW, warmup ratio 0.1, a linear learning-rate schedule, classifier-head learning rate $5E-4$, and batch size 32. Task-specific maximum sequence lengths and training epochs follow the PSOFT protocol.

Table 5: Shared hyperparameter settings for fine-tuning DeBERTaV3-base on the six-task GLUE setup.

Hyperparameter	CoLA	STS-B	MRPC	RTE	SST-2	QNLI
Optimizer			AdamW			
Warmup ratio			0.1			
LR schedule			Linear			
Learning rate (head)			$5E-4$			
Batch size			32			
Max seq. len.	64	128	256	256	128	256
#Epochs	20	20	30	30	10	5

LOFT variants. We evaluate three support families. $\text{LOFT}^{P_{\text{prin}}}$ uses the same principal right-singular support as PSOFT. $\text{LOFT}^{P_{\text{grad}}}$ uses a naive gradient-derived support obtained by collecting gradients on a short calibration set and taking the top- r right singular subspace of the resulting gradient matrix. $\text{LOFT}^{P_{\text{skew}}}$ uses the theory-guided support induced by $F = \text{skew}(W_0^\top G) = (W_0^\top G - G^\top W_0)/2$. For each support, we compare the default orthogonal transform $T_r = T_{\text{orth}}$ with a free variant $T_r = T_{\text{free}}$, where “free” denotes a fully unconstrained dense in-subspace transform initialized at the identity rather than a PSOFT-style easing factor.

Table 6: Task-specific learning rates for PSOFT and LOFT variants on the six-task GLUE setup.

Method	CoLA	STS-B	RTE	MRPC	SST-2	QNLI
PSOFT $_{r=46}$	6E-4	4E-4	4E-4	4E-4	2E-4	4E-4
LOFT $_{r=46}^{P_{\text{prin}}}$	6E-4	7E-4	9E-4	5E-4	9.5E-5	4.5E-4
LOFT $_{r=46}^{P_{\text{prin}}, T_{\text{free}}}$	1E-3	6E-4	7.5E-4	7E-4	6E-4	3E-4
LOFT $_{r=46}^{P_{\text{grad}}}$	5E-4	4E-4	1E-4	2E-4	4E-4	1E-4
LOFT $_{r=46}^{P_{\text{grad}}, T_{\text{free}}}$	5E-4	6E-4	1E-4	5E-4	6E-4	4E-4
LOFT $_{r=46}^{P_{\text{skew}}}$	5E-4	1E-4	5E-4	4E-4	2E-4	1E-4
LOFT $_{r=46}^{P_{\text{skew}}, T_{\text{free}}}$	5E-4	5E-4	1E-4	4E-4	2E-4	5E-4

E.2 Additional Follow-up on MNLI and QQP

MNLI-matched and QQP are reported as a secondary follow-up under the original GLUE development-set protocol, rather than as part of the primary six-task hold-out GLUE comparison. This distinction is important. The main GLUE table follows the PSOFT-style protocol on CoLA, STS-B, RTE, MRPC, SST-2, and QNLI: the original validation split is partitioned into a new validation split for model selection and a held-out test split for final reporting. By contrast, the MNLI/QQP follow-up reports performance directly on the standard GLUE development sets, matching the reporting convention used by the published DeBERTaV3-base baselines.

We use this setting because PSOFT does not report MNLI or QQP under its hold-out protocol, and reproducing a comparably controlled large-task hold-out benchmark would substantially increase computational cost. We therefore compare our finalized MNLI/QQP runs against the published DeBERTaV3-base development-set numbers reported in the corresponding original papers for LoRA, PiSSA, DoRA, LoRA-XS, BOFT, OFTv2/GOFTv2/qGOFTv2, and PSOFT (Hu et al., 2021; Meng et al., 2024; Liu et al., 2024a; Bałazy et al., 2024; Liu et al., 2024b; Qiu et al., 2025; Ma et al., 2024; Wu et al., 2026). This follow-up is consequently less controlled than the six-task hold-out benchmark, but it is useful for checking whether LOFT remains competitive on larger sentence-pair tasks under the widely used GLUE dev-set reporting protocol.

Protocol. Our runs use `microsoft/deberta-v3-base` with rank $r = 46$. We train with batch size 32, evaluate with batch size 64, use maximum sequence length 128, a linear learning-rate schedule, warmup ratio 0.1, and 10 training epochs. Evaluation is performed once per epoch, model selection uses development-set accuracy, and the best development checkpoint is loaded at the end. For MNLI, we report matched development accuracy only. Although the wrapper can evaluate both matched and mismatched splits, the finalized table uses MNLI-matched as the main MNLI metric and does not report mismatched accuracy.

Table 7: Shared hyperparameter settings for our MNLI-matched and QQP follow-up runs.

Hyperparameter	MNLI-matched	QQP
Backbone	DeBERTaV3-base	
Optimizer	AdamW	
Warmup ratio	0.1	
LR schedule	Linear	
Train batch size	32	
Eval batch size	64	
Max seq. len.	128	128
#Epochs	10	10
Model selection	Best validation accuracy	
Reported split	validation-matched	validation

Table 8: Follow-up results on MNLI-matched and QQP under the original GLUE development-set protocol. Baseline numbers are taken from the corresponding DeBERTaV3-base papers; our LOFT and PSOFT follow-up runs use train batch size 32, evaluation batch size 64, maximum sequence length 128, and 10 epochs. Results are averaged over five seeds where rerun by us.

Method	#Params	Mem.	MNLI-m	QQP	Avg.
FFT	184M	5.9	89.90	92.40	91.15
GOFV2	0.08M	18.5	90.10	90.85	90.48
qGOFV2	0.33M	18.5	90.17	91.34	90.76
BOFT $_{m=2}^{b=8}$	1.41M	6.3	90.25	92.10	91.18
OFTv2 $_{b=16}$	1.29M	4.5	90.33	92.10	91.22
LoRA $_{r=8}$	1.33M	4.5	90.65	91.99	91.32
PiSSA $_{r=8}$	1.33M	4.5	90.37	92.33	91.35
DoRA $_{r=16}$	1.41M	5.8	90.29	92.10	91.20
LoRA-XS $_{r=136}$	1.33M	4.2	OOM		N/A
PSOFT $_{r=46}$	0.08M	4.1	89.83	91.00	90.42
LOFT $_{r=46}^{P_{\text{prin}}}$	0.07M	4.1	90.12	91.05	90.58
LOFT $_{r=46}^{P_{\text{prin}}, T_{\text{free}}}$	0.15M	4.1	90.42	92.34	91.38
LOFT $_{r=46}^{P_{\text{skew}}}$	0.07M	4.1	90.35	92.13	91.24

Learning rates. For our MNLI/QQP runs, we swept learning rates in $\{1\text{E}-4, 2\text{E}-4, 3\text{E}-4, 5\text{E}-4, 7\text{E}-4, 1\text{E}-3\}$, depending on the variant. Table 9 lists the selected learning rates.

Table 9: Selected learning rates for our MNLI-matched and QQP follow-up runs.

Method	MNLI-matched	QQP
PSOFT $_{r=46}$	5E-4	5E-4
LOFT $_{r=46}^{P_{\text{prin}}}$	5E-4	5E-4
LOFT $_{r=46}^{P_{\text{prin}}, T_{\text{free}}}$	5E-4	5E-4
LOFT $_{r=46}^{P_{\text{skew}}}$	2E-4	3E-4

Interpretation. This follow-up should be read as a large-task sanity check rather than a fully controlled benchmark. The primary GLUE evidence in this paper remains the six-task hold-out comparison in Table 2, where all reported tasks follow the same PSOFT-style validation/test split protocol. MNLI and QQP are different: published DeBERTaV3-base baselines for these two tasks

are usually reported on the original GLUE development sets, and the corresponding papers do not use a single unified hyperparameter protocol. In particular, prior results differ in maximum sequence length, epoch count, dropout, batch size, and sometimes reuse numbers from earlier sources. Therefore, the MNLI/QQP table should not be interpreted as a strictly matched replacement for the main GLUE evaluation.

Despite this limitation, the follow-up is still informative because it tests whether the same LOFT design choices remain viable on larger sentence-pair datasets. Under the GLUE development-set reporting convention, $\text{LOFT}_{r=46}^{P_{\text{prin}}}$ recovers and improves over PSOFT, confirming that the principal-support LOFT implementation preserves the closest principal-subspace baseline behavior beyond the six-task hold-out setting. The free-transform variant $\text{LOFT}_{r=46}^{P_{\text{prin}}, T_{\text{free}}}$ achieves the strongest two-task average, showing that additional in-subspace flexibility can be helpful on large sentence-pair tasks. The SkewGrad variant $\text{LOFT}_{r=46}^{P_{\text{skew}}}$ remains competitive as well, although we treat the six-task hold-out results as the cleaner setting for isolating support-selection effects.

It is also worth noting that our MNLI/QQP runs use maximum sequence length 128. Some published DeBERTaV3-base GLUE baselines use longer task-specific maximum sequence lengths or otherwise different training recipes, so this follow-up is conservative with respect to input length and compute. The main takeaway is therefore not that the MNLI/QQP table establishes a fully controlled ranking across all methods, but that LOFT variants remain competitive under a widely used development-set protocol while using a relatively lightweight sequence-length configuration. We use these results as supportive evidence for scalability to larger GLUE tasks, while reserving Table 2 as the primary controlled GLUE conclusion.

E.3 VTAB-1K on ViT-B/16

Datasets and evaluation. We evaluate visual transfer on VTAB-1K, which consists of 19 tasks grouped into natural, specialized, and structured categories. Following the standard VTAB-1K protocol and PSOFT, each task uses 800 labeled training examples for adaptation and 200 validation examples for hyperparameter selection. Performance is reported as top-1 classification accuracy on the original test set. All numbers are averaged over five random seeds. Peak memory is measured on a single NVIDIA V100 64GB GPU.

Model and training protocol. We use ViT-B/16 as the image backbone. Unless otherwise stated, we use AdamW, warmup ratio 0.1, cosine learning-rate schedule, classifier-head learning rate $5\text{E}-3$, batch size 64, weight decay $1\text{E}-3$, dropout $1\text{E}-1$, and 50 epochs.

Table 10: Shared hyperparameter settings for fine-tuning ViT-B/16 on VTAB-1K.

Hyperparameter	ViT-B/16
Optimizer	AdamW
Warmup ratio	0.1
LR schedule	Cosine
Learning rate (head)	$5\text{E}-3$
Batch size	64
Weight decay	$1\text{E}-3$
Dropout	$1\text{E}-1$
#Epochs	50

LOFT variants on VTAB. We evaluate principal-support LOFT with orthogonal and free transforms at ranks $r = 42$ and $r = 46$. We additionally evaluate two orthogonal gradient-based variants: $\text{LOFT}^{P_{\text{grad}}}$ and $\text{LOFT}^{P_{\text{skew}}}$, both at rank $r = 46$. Table 11 reports the selected task-specific learning rates.

Table 11: Task-specific learning rates for LOFT variants on VTAB-1K. Task order follows the 19 VTAB tasks used in the main table.

Method	Cifar100	Caltech101	DTD102	Flower102	Pets	SVHN	Sun397	Camelion	EuroSAT	Resisc45	Retinopathy	Clevr-Count	Clevr-Dist	DMLab	KITTI-Dist	dSpr-Loc	dSpr-Ori	sNOIR-Azi	sNOIR-Ele
$\text{LOFT}_{r=42}^{P_{\text{prin}}}$	5E-4	3E-3	1E-3	2E-3	5E-4	3.5E-3	1.5E-3	5E-4	1.5E-3	2E-3	5E-4	1.5E-3	1E-3	3.5E-3	2E-3	3E-3	3.5E-3	5E-3	3.5E-3
$\text{LOFT}_{r=42}^{P_{\text{prin}}, T_{\text{free}}}$	1.5E-3	3.5E-3	1E-3	3.5E-3	5E-4	5E-3	1.5E-3	1E-3	3.5E-3	3.5E-3	1.5E-3	1.5E-3	5E-3	5E-3	3.5E-3	3.5E-3	1.5E-3	5E-3	3.5E-3
$\text{LOFT}_{r=46}^{P_{\text{prin}}}$	5E-4	4E-4	2E-4	1E-4	5E-4	3.5E-3	1.5E-3	1E-3	2E-3	2E-3	3E-3	1E-3	3.5E-3	3.5E-3	2E-3	3E-3	2E-3	3E-3	2E-3
$\text{LOFT}_{r=46}^{P_{\text{prin}}, T_{\text{free}}}$	1.5E-3	3.5E-3	5E-4	3.5E-3	5E-4	5E-3	1E-3	1E-3	3.5E-3	3.5E-3	1E-3	1E-3	5E-3	5E-3	3.5E-3	3.5E-3	1.5E-3	5E-3	1.5E-3
$\text{LOFT}_{r=46}^{P_{\text{grad}}}$	2E-4	9E-4	3.5E-4	3.5E-4	2.8E-4	9E-4	1.3E-3	7E-4	1.78E-3	9E-4	1.6E-4	7E-4	1.36E-3	1.73E-3	1.6E-3	4E-4	1.3E-3	1.73E-3	1.4E-3
$\text{LOFT}_{r=46}^{P_{\text{skew}}}$	1.5E-4	1.3E-3	2E-4	3E-4	4E-5	9.5E-4	2.9E-4	8E-4	8E-4	9E-4	7E-4	8E-4	8E-4	9E-4	8E-4	9E-4	9E-4	8E-4	9E-4

E.4 Mathematical Question Answering on MetaMathQA-40K

Datasets and evaluation. For mathematical reasoning, we fine-tune LLaMA2-7B on MetaMathQA-40K and evaluate the resulting models on GSM8K and MATH. This follows the standard mathematical reasoning protocol used in recent PEFT and orthogonal fine-tuning evaluations, where MetaMathQA-40K is used as the instruction-tuning set and GSM8K/MATH are used as held-out reasoning benchmarks. All methods are evaluated under the same finalized pipeline to avoid method-dependent differences in answer parsing, adapter loading, or post-training deployment.

For GSM8K, we report exact-match accuracy after extracting the final numerical answer from model generations. For MATH, we use the same corrected answer-extraction routine across all methods and report the final accuracy on the evaluation set. In both benchmarks, all finalized PEFT adapters are trained first and merged only after training before evaluation. This avoids discrepancies caused by evaluating unmerged adapters or by merging adapters at different stages of training.

For evaluation throughput, we use batch size 32 on GSM8K and batch size 1 on MATH. Unless otherwise stated, all methods are evaluated on a single NVIDIA A100-SXM GPU. HRA is evaluated on a single NVIDIA H200-SXM GPU because its implementation incurs a substantially larger memory requirement and does not fit under the same A100 setting used by the other methods.

Low-budget adaptation setting. The main mathematical reasoning comparison is designed as a matched low-budget experiment. Instead of comparing methods at the larger parameter scale used in prior full-budget PEFT tables, we restrict all main methods to approximately 0.5M trainable parameters. This setting makes the comparison more diagnostic: it tests whether the method can use a very small adaptation budget effectively, rather than simply benefiting from a larger number of trainable parameters.

For LoRA, we use rank $r = 1$, which gives 0.524M trainable parameters in this setting. For PSOFT and LOFT, we use rank $r = 128$, resulting in approximately 0.52–0.54M trainable parameters. This is possible because LOFT and PSOFT place the trainable transformation inside a compact subspace rather than training two full low-rank factors. For BOFT and HRA, we use their closest low-budget configurations that remain comparable in parameter count.

Training protocol. All memory-feasible methods are fine-tuned with the same general training protocol. We use AdamW, cosine learning-rate decay, warmup ratio 0.1, maximum sequence length

512, train batch size 64, and 2 training epochs. Method-specific differences are limited to the adapter parameterization, rank/configuration, learning rate, and support selection rule. The finalized learning rate for each method is reported in Table 13.

Table 12: Shared hyperparameter settings for low-budget MetaMathQA-40K fine-tuning.

Hyperparameter	Value
Base model	LLaMA2-7B
Training data	MetaMathQA-40K
Evaluation datasets	GSM8K, MATH
Optimizer	AdamW
Warmup ratio	0.1
LR schedule	Cosine
Max sequence length	512
Train batch size	64
Training epochs	2
GSM8K eval batch size	32
MATH eval batch size	1
Default GPU	NVIDIA A100-SXM
HRA GPU	NVIDIA H200-SXM

Compared methods. We compare LOFT against representative low-rank and orthogonal PEFT baselines under the matched low-budget setting.

- **LoRA** uses a rank-1 additive low-rank update.
- **BOFT** uses the low-budget butterfly orthogonal configuration $b = 2, m = 1$.
- **HRA** uses Householder Reflection Adaptation with $r = 2$ and strict orthogonality, i.e., $\lambda = \infty$.
- **PSOFT** uses principal-subspace orthogonal fine-tuning with rank $r = 128$.
- **Ortho LOFT-prin** uses the same orthogonal LOFT parameterization with principal support.
- **Ortho LOFT-GradSVD** selects the support using gradient singular directions.
- **Ortho LOFT-SkewGrad** selects the support from skew-gradient information.

The principal LOFT variant is included to isolate the effect of the parameterization when the support is chosen from pretrained weight geometry. The GradSVD and SkewGrad variants are included to test whether task-informed support selection improves mathematical reasoning under the same parameter budget.

Learning rates and method configurations. Table 13 reports the finalized learning rates and parameter budgets used in the low-budget mathematical reasoning experiments. The learning rate is tuned per method, while the trainable parameter count is kept close to 0.5M whenever possible.

Table 13: Method-specific settings for low-budget MetaMathQA-40K fine-tuning.

Method	Configuration	#Params	Learning rate
BOFT	$b = 2, m = 1$	0.786M	$8E-4$
LoRA	$r = 1$	0.524M	$8E-4$
HRA	$r = 2, \lambda = \infty$	0.524M	$1E-3$
PSOFT	$r = 128$	0.536M	$5E-4$
Ortho LOFT-prin	$r = 128$	0.520M	$5E-4$
Ortho LOFT-GradSVD	$r = 128$	0.520M	$8E-4$
Ortho LOFT-SkewGrad	$r = 128$	0.520M	$8E-4$

Peak memory measurement. The memory column in Table 3 reports peak GPU memory allocated during training. For each method, we reset the CUDA peak-memory counter before fine-tuning and record the maximum allocated memory reached under the shared training pipeline. All memory-feasible methods are run on a single NVIDIA A100-SXM GPU. HRA is run on a single NVIDIA H200-SXM GPU due to out-of-memory issues on A100-SXM.

Under this measurement, LoRA and PSOFT require 49.50GB and 28.67GB, respectively, while all LOFT variants require 25.68GB. Thus, LOFT has the lowest peak memory among the compared methods, reducing memory by 48.1% relative to LoRA and 10.4% relative to PSOFT. BOFT and HRA require 63.24GB and 124.92GB, respectively, corresponding to 59.4% and 79.4% reductions for LOFT in our implementation.

Evaluation implementation details. We found mathematical reasoning evaluation to be sensitive to two implementation details. First, answer extraction can noticeably affect GSM8K and MATH scores if the parser only recognizes overly restrictive numerical formats. We therefore use a corrected answer-extraction routine that handles more general numeric patterns and apply it consistently to all finalized methods. Second, adapter deployment timing can affect the final reported score. In the finalized pipeline, each adapter is trained to completion, then merged into the backbone only after training, and the merged model is used for evaluation. This ensures that the reported differences reflect the adaptation method rather than inconsistencies in adapter loading or merging.

Result summary. Table 3 reports the final GSM8K and MATH results. The principal-support LOFT variant performs similarly to PSOFT, which is expected because both rely on pretrained weight geometry to define the adaptation support. However, replacing principal support with gradient-informed support substantially improves the accuracy-memory trade-off. GradSVD achieves the best GSM8K result, while SkewGrad achieves the best MATH result, both under the same $r = 128$ and approximately 0.52M-parameter budget. These results show that, in the low-budget decoder-side setting, the main benefit of LOFT comes not only from operating in a compact subspace, but from selecting a support that is better aligned with task-specific optimization geometry.

F Full Short-Horizon Support Diagnostics

This appendix provides the full numerical results for short-horizon diagnostics of the first-order support-selection mechanism. These diagnostics are not intended to replace final task evaluation. Instead, they test a narrower initialization-local question: whether the support score predicted by Proposition 2 identifies subspaces that expose useful short-horizon descent directions. We report two complementary diagnostics. The first is a controlled probe diagnostic, where supports are

constructed from training-only calibration batches, the task head and all non-LOFT parameters are frozen, and only the LOFT adapter is updated for a small number of steps. This setting isolates the effect of the selected support. The second is an early-validation diagnostic under the standard GLUE training pipeline, where the LOFT adapter and task head are updated while the pretrained backbone remains frozen, and validation loss is recorded during the first 25 update steps.

GradSVD is included here as an auxiliary gradient-informed baseline. It selects a support from the principal right singular subspace of the downstream gradient, but unlike SkewGrad it does not follow the skew-symmetric first-order generator $F = \text{skew}(W_0^\top G)$ that governs orthogonal subspace adaptation. Its role is therefore diagnostic: it tests whether generic gradient awareness is sufficient, or whether the orthogonal-specific skew signal is needed.

F.1 Does the First-Order Signal Predict Support Quality?

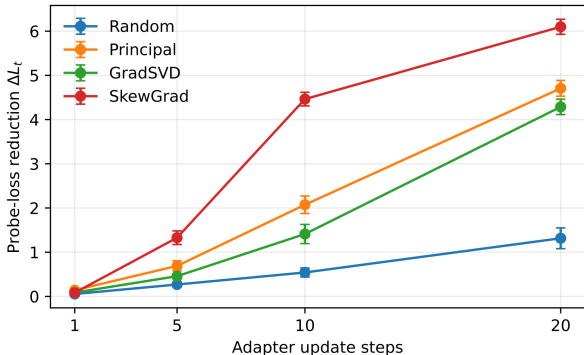
We first define the support score used in the diagnostics. The first-order analysis gives a criterion for choosing the support before training, and the experiments below test whether this criterion aligns with short-horizon optimization behavior. For each adapted layer ℓ , let $F_\ell = \text{skew}(W_{0,\ell}^\top G_\ell)$, where G_ℓ is the calibration gradient at initialization. Given a chosen support $P = \{P_{r,\ell}\}_{\ell \in \mathcal{L}}$, define its relative signal capture as

$$\rho(P) = \frac{\sum_{\ell \in \mathcal{L}} \|P_{r,\ell} F_\ell P_{r,\ell}^\top\|_F^2}{\sum_{\ell \in \mathcal{L}} 2 \sum_{k=1}^{r/2} \mu_{\ell,k}^2},$$

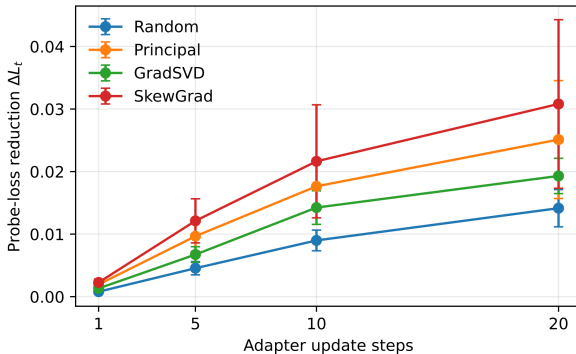
where $\{\pm i\mu_{\ell,k}\}$ are the skew-eigenvalue pairs of F_ℓ , ordered by $\mu_{\ell,1} \geq \mu_{\ell,2} \geq \dots$. The denominator is the best rank- r skew-invariant signal predicted by Proposition 2. Thus, SkewGrad has $\rho(P) \approx 1$ on the calibration batches by construction. The key question is whether this local score also predicts short-horizon loss decrease.

Random support serves as a task-agnostic control: if any low-dimensional support were sufficient, Random would be competitive. Principal support tests whether pretrained-weight geometry alone is sufficient, while GradSVD and SkewGrad test two ways of using downstream gradient information.

Controlled probe diagnostic. Figure 4 and Table 14 report the full controlled probe diagnostic with Random, Principal, GradSVD, and SkewGrad supports. The score $\rho(P)$ is the relative calibration skew-signal capture defined above. Because SkewGrad is constructed from the top skew-invariant subspace, it achieves $\rho(P) \approx 1$ on the calibration gradients by construction. The important question is whether this local signal translates into short-horizon loss decrease on held-out probe batches.



(a) STS-B.



(b) CoLA.

Figure 4: **All-support controlled probe diagnostic.** The task head and all non-LOFT parameters are frozen, so the probe-loss reduction isolates the effect of support selection. GradSVD is included as a gradient-only auxiliary baseline. Compared with GradSVD, SkewGrad better matches the orthogonal first-order generator $F = \text{skew}(W_0^\top G)$, and yields the strongest short-horizon probe-loss reduction on both tasks.

Table 14: **Full controlled probe diagnostics.** Mean \pm standard deviation over five seeds. $\rho(P)$ is relative calibration skew-signal capture, and ΔL_t is probe-loss reduction after t adapter-update steps. The task head and all non-LOFT parameters are frozen.

(a) STS-B					
Support	$\rho(P)$	ΔL_1	ΔL_5	ΔL_{10}	ΔL_{20}
Random	0.0020 \pm 0.0003	0.055 \pm 0.007	0.269 \pm 0.106	0.541 \pm 0.226	1.315 \pm 0.526
Principal	0.0357 \pm 0.0070	0.140 \pm 0.026	0.690 \pm 0.261	2.073 \pm 0.443	4.707 \pm 0.400
GradSVD	0.0491 \pm 0.0073	0.087 \pm 0.008	0.457 \pm 0.133	1.411 \pm 0.485	4.287 \pm 0.390
SkewGrad	1.0000 \pm 0.0000	0.083 \pm 0.038	1.328 \pm 0.343	4.463 \pm 0.345	6.099 \pm 0.383

(b) CoLA					
Support	$\rho(P)$	ΔL_1	ΔL_5	ΔL_{10}	ΔL_{20}
Random	0.0020 \pm 0.0004	0.0008 \pm 0.0003	0.0045 \pm 0.0024	0.0090 \pm 0.0037	0.0141 \pm 0.0067
Principal	0.0353 \pm 0.0153	0.0020 \pm 0.0014	0.0097 \pm 0.0053	0.0176 \pm 0.0082	0.0251 \pm 0.0211
GradSVD	0.0500 \pm 0.0052	0.0013 \pm 0.0006	0.0067 \pm 0.0028	0.0142 \pm 0.0060	0.0193 \pm 0.0063
SkewGrad	0.9995 \pm 0.0001	0.0023 \pm 0.0012	0.0121 \pm 0.0079	0.0216 \pm 0.0202	0.0308 \pm 0.0301

The controlled probe results confirm the predicted ordering. On STS-B, SkewGrad gives the strongest reduction from step 5 onward and the largest reduction at step 20. On CoLA, SkewGrad gives the largest mean reduction across all measured steps, although the results have higher variance. GradSVD captures more skew-signal than Random but does not match SkewGrad, suggesting that generic gradient awareness is less effective than the orthogonal-specific skew signal.

Practical significance. The controlled probe diagnostic is not intended to replace final validation or test performance. Its practical role is to provide a cheap, calibration-stage test of whether a candidate support exposes useful local descent directions before running full fine-tuning. This is especially relevant in step-limited adaptation settings, such as rapid personalization, low-resource task adaptation, or federated/local fine-tuning, where the first few update steps can matter disproportionately. The comparison with GradSVD also shows that generic gradient information is not sufficient: aligning the support with the skew-symmetric generator specific to orthogonal adaptation gives a stronger short-horizon optimization signal.

Calibration-size robustness. We additionally vary the number K of training-only calibration mini-batches used to construct the SkewGrad support. This diagnostic tests whether SkewGrad depends on a large auxiliary calibration set, while keeping the rank, transform class, optimizer, and probe protocol fixed. Since $\rho(P)$ is measured on the calibration skew signal used for support construction, it mainly serves as a construction-stability check. The more important quantity is the controlled probe loss reduction ΔL_{20} , which tests whether the constructed support yields useful short-horizon optimization. The results show that small calibration sizes are already sufficient: $K = 1$ or $K = 2$ achieves near-saturated $\rho(P)$ on most tasks and competitive ΔL_{20} across tasks.

Increasing K does not systematically improve the probe objective, suggesting that SkewGrad does not rely on a large hidden calibration set.

Table 15: **Calibration-size robustness for SkewGrad.** K is the number of training-only calibration mini-batches used to construct the SkewGrad support. Values are mean \pm standard deviation over five seeds. Rank, transform, optimizer, and probe protocol are fixed. ΔL_{20} is the controlled probe-loss reduction after 20 adapter-update steps.

Task	K	$\rho(P)$	ΔL_{20}
CoLA	1	0.9991 ± 0.0002	0.1133 ± 0.0466
CoLA	2	0.9991 ± 0.0001	0.0740 ± 0.0415
CoLA	4	0.9995 ± 0.0001	0.0308 ± 0.0270
CoLA	8	0.9993 ± 0.0002	0.0310 ± 0.0195
MRPC	1	0.9902 ± 0.0034	0.1623 ± 0.0154
MRPC	2	0.9978 ± 0.0010	0.1845 ± 0.0315
MRPC	4	0.9994 ± 0.0002	0.1417 ± 0.0164
MRPC	8	0.9998 ± 0.0000	0.0870 ± 0.0306
STS-B	1	0.9999 ± 0.0000	8.3965 ± 0.3313
STS-B	2	0.9999 ± 0.0000	7.4750 ± 0.5630
STS-B	4	1.0000 ± 0.0000	6.0991 ± 0.3423
STS-B	8	1.0000 ± 0.0000	3.4890 ± 0.3343

Table 15 shows that SkewGrad does not require a large calibration set to construct a useful support. The calibration skew-signal capture $\rho(P)$ is already close to one with $K = 1$ on CoLA and STS-B, and reaches the same near-saturated regime on MRPC with $K = 2$ or $K = 4$. The probe-loss reduction also remains strong with small K : on MRPC and STS-B, SkewGrad gives the largest ΔL_{20} among Random, Principal, GradSVD, and SkewGrad for all tested calibration sizes; on CoLA, it is strongest for $K \leq 4$, while the $K = 8$ differences are small and within the high variance of the task. These results suggest that the proposed support construction is not dependent on a large auxiliary calibration set; a few training-only mini-batches are sufficient for the short-horizon optimization signal used by SkewGrad.

Early validation diagnostic. The early-validation curves and summary statistics are reported in Figure 5 and Table 16. This diagnostic checks whether the short-horizon ordering observed in the controlled probe setting is also visible under the standard GLUE training pipeline. The LOFT adapter and task head are updated while the pretrained backbone remains frozen, and validation loss is recorded at fixed early update steps. We use these results only as a sanity check for early training behavior; they are not intended to replace final task performance.

Table 16: **Early validation loss.** Mean \pm standard deviation over five seeds. Validation loss is recorded at fixed update steps in the first 25 training steps. Average loss is computed over the listed step ranges. Wins count how many fixed steps give the lowest mean validation loss. Lower loss and more wins are better.

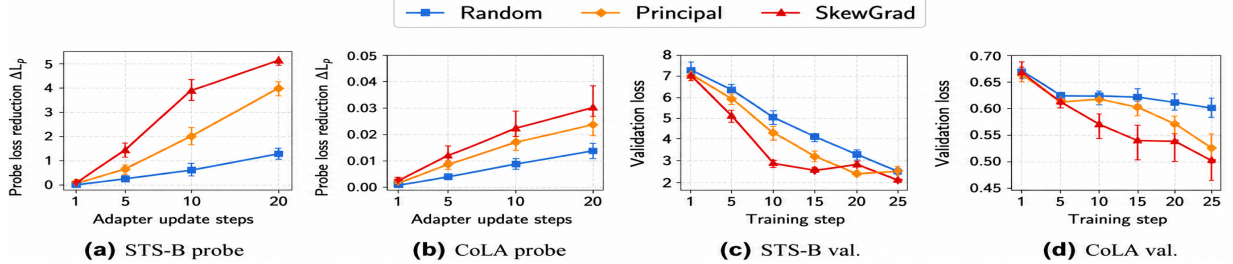


Figure 5: **Short-horizon support diagnostics.** Panels (a,b) show held-out probe-loss reduction after adapter-only updates. Panels (c,d) show validation loss during the first 25 steps of normal GLUE training. All panels compare Random, Principal, and SkewGrad under matched rank, optimizer, learning rate, and orthogonal LOFT transform. GradSVD is included in the full controlled-probe results in Table 14.

Task	Support	Avg. loss 5–20	Avg. loss 5–25	Wins 1–25	Wins 5–25
STS-B	Random	4.5900 ± 0.3400	4.1745 ± 0.2927	0	0
	Principal	3.9261 ± 0.3246	3.6557 ± 0.2289	2	1
	SkewGrad	3.4281 ± 0.2808	3.1687 ± 0.2911	4	4
CoLA	Random	0.6235 ± 0.0163	0.6200 ± 0.0160	0	0
	Principal	0.6026 ± 0.0206	0.5866 ± 0.0218	1	0
	SkewGrad	0.5673 ± 0.0346	0.5570 ± 0.0419	5	5

The early-validation results show that the same ordering also appears in normal GLUE training. Within the first 25 updates, SkewGrad achieves the lowest average validation loss on both tasks and wins most fixed horizons. This supports the narrower claim that the score in Proposition 2 identifies supports that help early optimization. Together with the controlled probe and calibration-size diagnostics, these results link the first-order support signal to short-horizon descent behavior under matched rank, optimizer, and transform settings.

G Full Support and Transform Ablations

This appendix reports LOFT variants omitted from the main GLUE and VTAB tables. For these two benchmarks, the main text fixes the default orthogonal transform $T_r = T_{\text{orth}}$ and focuses on principal support $P_r = P_{\text{prin}}$ and SkewGrad support $P_r = P_{\text{skew}}$. Here we additionally report GradSVD support $P_r = P_{\text{grad}}$, unconstrained transform variants $T_r = T_{\text{free}}$, and auxiliary rank variants whenever available. Some rows are repeated from the main text so that each benchmark has a complete ablation table in one place. After each table, we summarize which effects are attributable to support selection and which are attributable to the transform class.

GLUE ablations. Table 17 reports the full GLUE table, including OOM baselines, GradSVD supports, and free in-subspace transforms. The main text reports only the default orthogonal transform and the two support choices most relevant to the main mechanism.

Table 17: Full results on six controlled GLUE tasks using DeBERTaV3-base under the same hold-out validation protocol as PSOFT. We report Matthews correlation on CoLA, Pearson correlation on STS-B, and accuracy on RTE, MRPC, SST-2, and QNLI. All results are averaged over five random seeds. Peak memory is measured on a single NVIDIA V100 64GB GPU. For LOFT, the subscript denotes rank r , the superscript denotes support P_r , and $T_r = T_{\text{orth}}$ is used by default unless $T_r = T_{\text{free}}$ is shown.

Method	#Params	Mem. (GB)	CoLA	STS-B	RTE	MRPC	SST-2	QNLI	Avg.
FFT	184M	5.9	67.56	91.46	82.88	90.69	94.13	93.37	86.68
GOFTv2	0.08M	18.5	65.45			OOM			N/A
qGOFTv2	0.33M	18.5	68.03			OOM			N/A
BOFT $_{m=2}^{b=8}$	1.41M	6.3	68.85	91.09	83.60	88.40	95.28	93.78	86.83
OFTv2 $_{b=32}$	1.29M	4.5	66.79	91.22	84.03	89.61	93.72	92.64	86.34
LoRA $_{r=8}$	1.33M	4.5	67.98	91.60	84.87	90.20	95.28	93.89	87.30
PiSSA $_{r=8}$	1.33M	4.5	66.50	91.40	83.77	89.90	93.17	92.72	86.24
DoRA $_{r=8}$	1.41M	5.8	67.06	91.60	87.19	90.49	95.23	94.09	87.61
LoRA-XS $_{r=136}$	1.33M	4.2	64.67	91.48	84.17	91.27	93.85	93.14	86.43
PSOFT $_{r=46}$	0.08M	4.1	70.42	91.56	86.74	90.49	95.55	93.47	88.04
LOFT $_{r=46}^{P_{\text{prin}}}$	0.07M	4.1	70.52	91.37	86.19	90.90	95.73	93.63	88.06
LOFT $_{r=46}^{P_{\text{prin}}, T_{\text{free}}}$	0.15M	4.1	70.84	91.41	87.05	91.17	95.41	94.23	88.35
LOFT $_{r=46}^{P_{\text{grad}}}$	0.07M	4.1	70.63	91.32	87.05	91.67	95.28	94.39	88.39
LOFT $_{r=46}^{P_{\text{grad}}, T_{\text{free}}}$	0.15M	4.1	72.09	91.58	86.17	91.18	95.24	93.45	88.29
LOFT $_{r=46}^{P_{\text{skew}}}$	0.07M	4.1	72.03	91.75	86.83	92.36	95.42	93.97	88.73
LOFT $_{r=46}^{P_{\text{skew}}, T_{\text{free}}}$	0.15M	4.1	71.04	91.50	86.77	92.65	94.72	94.43	88.52

Table 18: Task-specific standard deviations for LOFT variants on the six-task GLUE setup. Values are standard deviations over five random seeds and use the same task order as Table 17.

Method	CoLA	STS-B	RTE	MRPC	SST-2	QNLI
LOFT $_{r=46}^{P_{\text{prin}}}$	1.13	0.32	1.58	1.71	0.31	0.25
LOFT $_{r=46}^{P_{\text{prin}}, T_{\text{free}}}$	1.12	0.26	2.83	1.22	0.35	0.31
LOFT $_{r=46}^{P_{\text{grad}}}$	1.11	0.48	3.35	1.65	0.16	0.25
LOFT $_{r=46}^{P_{\text{grad}}, T_{\text{free}}}$	1.81	0.38	2.74	2.97	0.82	0.62
LOFT $_{r=46}^{P_{\text{skew}}}$	1.85	0.38	3.43	1.50	0.38	0.46
LOFT $_{r=46}^{P_{\text{skew}}, T_{\text{free}}}$	2.53	0.39	2.62	2.06	0.91	0.37

GLUE ablation analysis. The full GLUE ablation separates the two LOFT design axes. Under the default orthogonal transform, changing the support gives a clear ordering: LOFT $_{r=46}^{P_{\text{prin}}}$ reaches 88.06, LOFT $_{r=46}^{P_{\text{grad}}}$ improves to 88.39, and LOFT $_{r=46}^{P_{\text{skew}}}$ further improves to 88.73. This shows that generic gradient awareness is useful, but the orthogonal-specific skew-gradient signal gives the strongest support.

The transform-class comparison is more nuanced. The free transform helps in the principal-support regime, improving LOFT $_{r=46}^{P_{\text{prin}}}$ from 88.06 to 88.35, but it is not uniformly better than the orthogonal transform. For GradSVD, the orthogonal and free variants are close in average score, 88.39 versus 88.29. For SkewGrad, the orthogonal transform remains stronger than the free

transform, 88.73 versus 88.52. These results suggest that, on GLUE, the primary gain comes from selecting a better task-aligned support, while orthogonality remains a useful regularizer once the support is already informative. The OOM rows for GOFTv2/qGOFTv2 further indicate that the comparison is constrained by practical memory feasibility, not only by final accuracy.

Table 18 reports the corresponding across-seed standard deviations for the LOFT rows. The variance is largest on small or seed-sensitive tasks such as RTE and CoLA, while STS-B, SST-2, and QNLI are comparatively stable across seeds. The strongest average result, $\text{LOFT}_{r=46}^{P_{\text{skew}}}$, is therefore not an isolated transform-class effect: it combines the most informative support with the regularity of the orthogonal in-subspace transform.

VTAB ablations. Table 19 reports the full 19-task VTAB-1K results, including auxiliary LOFT support and transform variants omitted from the main text.

Table 19: Full VTAB-1K results of fine-tuned ViT-B/16. Reported values are top-1 accuracy (%) averaged over five random seeds. We report trainable parameter count and peak memory to show the efficiency–performance trade-off across PEFT methods. For LOFT, the subscript denotes rank r , the superscript denotes support P_r , and $T_r = T_{\text{orth}}$ is used by default unless $T_r = T_{\text{free}}$ is shown.

Method	#Params	Mem.	Natural						Specialized				Structured						Avg.			
			Cifar100	Caltech101	DTD102	Flower102	Pets	SVHN	Sun397	Camelyon	EuroSAT	Resisc45	Retinopathy	Clevr-Count	Clevr-Dist	DMLab	KITTI-Dist	dSpr-Loc		dSpr-Ori	sNORB-Azi	sNORB-Ele
FFT	85.9M	8.2	70.7	89.3	69.5	99.0	90.4	81.7	54.9	85.4	93.6	83.8	74.5	58.3	51.5	43.2	75.0	73.1	48.7	16.4	30.0	67.8
GOFTv2	0.08M	OOM																				
qGOFTv2	0.33M	OOM																				
BOFT $_{n=2}^{b=8}$	1.41M	10.9	70.6	88.2	69.8	99.0	91.4	77.4	55.1	85.1	93.6	82.3	74.9	61.8	50.4	42.9	76.1	73.7	48.8	15.7	30.8	70.9
OFTv2 $_{b=32}$	1.29M	7.7	68.5	88.9	67.5	98.4	89.5	86.9	53.6	86.0	94.1	84.2	74.6	58.7	56.4	46.7	78.5	81.1	48.1	17.3	32.5	72.1
LoRA $_{r=8}$	1.33M	9.9	71.4	88.4	70.1	99.0	91.4	76.6	55.7	85.9	94.2	83.3	74.1	72.0	54.3	43.0	76.6	74.8	48.6	16.4	31.8	71.8
PiSSA $_{r=8}$	1.33M	9.9	70.7	88.7	68.9	99.2	91.0	81.9	53.3	82.6	93.4	83.0	74.0	71.0	60.2	44.0	77.1	81.9	51.8	18.1	33.1	72.3
DoRA $_{r=8}$	1.41M	17.8	70.7	89.0	69.8	98.9	91.0	81.7	55.5	85.7	94.2	83.5	74.8	67.3	54.2	45.1	77.4	82.0	48.5	16.9	31.5	72.3
LoRA-XS $_{r=136}$	1.33M	6.6	68.5	89.4	68.4	98.7	90.9	84.5	54.1	84.0	94.3	80.8	73.6	60.0	57.7	45.8	79.6	80.6	48.1	17.4	30.8	71.6
PSOFT $_{r=46}$	0.08M	6.2	71.9	89.6	70.3	99.1	91.8	86.9	55.9	84.6	94.2	82.4	75.2	71.2	59.9	45.7	79.6	80.9	52.9	20.0	32.9	73.4
LOFT $_{P_{r=42}}^{P_{\text{prin}}}$	0.06M	5.7	70.3	90.1	69.2	99.1	91.1	86.0	54.9	86.5	94.5	83.8	75.3	70.9	59.9	45.0	79.6	79.5	51.8	19.9	32.6	73.4
LOFT $_{P_{r=42}}^{P_{\text{prin}}, T_{\text{free}}}$	0.13M	5.7	70.2	90.5	70.0	99.2	91.5	86.2	55.2	86.3	94.7	83.5	75.2	68.7	60.1	46.1	79.7	79.7	50.6	19.9	32.1	73.3
LOFT $_{P_{r=46}}^{P_{\text{prin}}}$	0.07M	5.7	68.0	89.5	69.1	99.1	91.2	86.1	54.5	85.0	94.3	80.7	75.3	65.2	58.0	45.2	79.2	79.4	48.3	19.5	31.7	72.3
LOFT $_{P_{r=46}}^{P_{\text{prin}}, T_{\text{free}}}$	0.15M	5.7	69.1	89.8	69.5	99.1	91.5	86.2	54.9	84.9	94.3	81.5	74.9	67.3	56.8	45.6	77.0	79.2	48.1	19.0	30.8	72.3
LOFT $_{P_{r=46}}^{\text{grad}}$	0.07M	5.7	69.9	89.6	69.4	99.2	92.0	85.2	55.2	86.4	95.7	82.7	75.3	68.9	59.8	46.2	79.8	79.8	50.2	19.8	33.2	73.3
LOFT $_{r=46}^{\text{skew}}$	0.07M	5.7	71.8	90.1	70.2	99.3	92.1	86.2	55.7	86.7	95.0	83.7	75.5	71.2	59.9	46.1	80.1	80.1	52.5	20.0	33.1	73.8

Table 20: Task-specific standard deviations for selected LOFT variants on VTAB-1K. Values are reported in percentage points and computed over five random seeds. We report the main principal-support row, its free-transform counterpart, and the two gradient-informed orthogonal supports used in the VTAB ablation.

Method	Cifar100	Caltech101	DTD102	Flower102	Pets	SVHN	Sun397	Camelyon	EuroSAT	Resisc45	Retinopathy	Clevr-Count	Clevr-Dist	DMLab	KITTI-Dist	dSpr-Loc	dSpr-Ori	sNORB-Azi	sNORB-Ele
LOFT $_{P_{r=42}}^{P_{\text{prin}}}$	1.91	0.74	0.32	0.20	0.13	0.92	0.64	0.22	0.18	1.24	0.48	2.25	0.52	0.41	1.75	0.36	1.68	0.72	0.66
LOFT $_{P_{r=42}}^{P_{\text{prin}}, T_{\text{free}}}$	1.43	0.77	0.70	0.16	0.40	0.19	0.85	0.93	0.59	1.19	0.29	2.55	0.66	0.68	1.40	0.34	3.27	1.57	1.09
LOFT $_{P_{r=46}}^{\text{grad}}$	0.23	0.19	0.14	0.02	0.20	0.22	0.13	0.17	0.04	0.34	0.68	1.93	0.55	0.20	0.72	0.39	0.34	0.23	0.53
LOFT $_{r=46}^{\text{skew}}$	0.18	0.22	0.25	0.08	0.37	0.32	0.11	0.38	0.15	0.29	0.28	1.50	0.45	0.39	0.42	0.51	0.68	0.32	0.48

VTAB ablation analysis. The VTAB ablation shows a more heterogeneous pattern than GLUE, which is expected because VTAB aggregates natural, specialized, and structured visual tasks. The $r = 42$ principal-support row is the most direct recovery of the PSOFT regime: $\text{LOFT}_{r=42}^{P_{\text{prin}}}$ matches PSOFT’s average while using fewer parameters and less memory. Increasing the principal rank to $r = 46$ does not improve the average, indicating that simply increasing the subspace width is not sufficient. GradSVD gives strong task-level results on several datasets, such as Flower102, Pets, EuroSAT, and sNORB-Ele, but its average remains below SkewGrad. The best overall average is obtained by $\text{LOFT}_{r=46}^{P_{\text{skew}}}$, which reaches 73.8 and improves over both PSOFT and the principal-support LOFT variants. This comparison is especially informative because the $r = 46$ principal-support rows do not improve over the $r = 42$ principal-support row, whereas the SkewGrad support at $r = 46$ gives the strongest average. Thus, the improvement is better explained by support selection than by simply increasing rank. The result supports the same qualitative conclusion as GLUE: generic gradient awareness helps, but the orthogonal-specific skew-gradient support is the most reliable support choice. Free-transform variants do not improve the VTAB average, suggesting that visual transfer benefits more from support selection than from relaxing the in-subspace orthogonality constraint. Table 20 reports the corresponding across-seed variability for selected LOFT variants. The gradient-informed supports are generally stable: the average task-level standard deviation is about 0.38 percentage points for $P_r = P_{\text{grad}}$ and 0.39 percentage points for $P_r = P_{\text{skew}}$. The largest variances occur on a small number of structured tasks, especially Clevr-Count and dSpr-Ori, while most natural and specialized tasks have substantially smaller variation. This helps rule out the concern that the VTAB average gain is driven by highly unstable seed behavior, although we still interpret the VTAB improvement as modest rather than uniform across all tasks.

H Additional Robustness Analyses

H.1 Low-Resource Language OOD Adaptation

We further evaluate whether gradient-informed support selection remains effective in a low-resource language adaptation setting. We fine-tune Llama-3.2-3B on Bactrian-X and report held-out response-only negative log-likelihood (NLL). We use the base-model bits-per-byte (BPB) on held-out raw text as a rough proxy for language OOD strength. The shared experimental setup is summarized in Table 21.

Table 21: Shared hyperparameter settings for low-resource language adaptation.

Hyperparameter	Value
Base model	Llama-3.2-3B
Training data	Bactrian-X, 5,000 examples per language
Hold-out data	500 examples per language
Evaluation metric	Response-only NLL ↓
OOD proxy	Base-model BPB on held-out raw text
Optimizer	AdamW
Learning-rate schedule	Cosine, warmup ratio 0.1
Default learning rate	2×10^{-4}
Weight decay	0.0
Training epochs	2
Batch size	1
Gradient accumulation	64
Precision	bf16
Seeds	0, 1, 2
LOFT / PSOFT rank	354
Gradient calibration	16 examples
PSOFT extras	Magnitude vectors and Cayley–Neumann approximation with 5 terms

Table 22: Low-resource language adaptation on Bactrian-X. We report held-out response-only NLL (lower is better), averaged over three seeds. All methods use learning rate 2×10^{-4} . BPB is measured before fine-tuning and serves as an approximate OOD-strength proxy.

Method	Indonesian (id)	English (en)	Tagalog (tl)	Afrikaans (af)	Swahili (sw)	Avg.
BPB	0.596	0.626	0.811	0.831	1.065	–
Principal	1.0556	1.8715	1.3771	1.3513	1.3631	1.4037
GradSVD	1.0553	1.8655	1.3708	1.3463	1.3480	1.3972
SkewGrad	1.0666	1.9037	1.3768	1.3585	1.3503	1.4112
PSOFT	1.0557	1.8747	1.3770	1.3511	1.3628	1.4043

Table 22 shows that the gradient-informed support generally improves over the principal weight-based support in this OOD adaptation setting. The gain is small when the base model is already close to the target language distribution, such as Indonesian, but becomes much larger for the strongest OOD language, Swahili. PSOFT closely tracks the principal support, which is expected because both choose the adaptation support from pretrained-weight geometry rather than from downstream gradient information. SkewGrad is less stable: it helps on Swahili but degrades performance on Indonesian, English, and Afrikaans, suggesting that mixing pretrained-weight geometry into the skew signal can be harmful when pretrained directions are already well aligned with the task.

To check that the GradSVD advantage is not an artifact of a single learning rate, we run an extended learning-rate sweep on Swahili, the strongest OOD language in this set. We also include a parameter-matched LoRA baseline and a half-parameter tier.

Table 23: Swahili learning-rate and parameter-budget ablation. We report each method at its own best learning rate. The 12M tier compares LOFT/PSOFT rank 354 with LoRA rank 8; the 6M tier compares LOFT/PSOFT rank 250 with LoRA rank 4.

Method	12M tier		6M tier	
	Best lr	NLL ↓	Best lr	NLL ↓
Principal	5×10^{-4}	1.3307	1×10^{-3}	1.3546
GradSVD	5×10^{-4}	1.3170	1×10^{-3}	1.3395
SkewGrad	3×10^{-4}	1.3399	5×10^{-4}	1.3697
PSOFT	5×10^{-4}	1.3300	1×10^{-3}	1.3534
LoRA	1×10^{-3}	1.3362	1×10^{-3}	1.3646

Table 23 confirms that LOFT’s gradient-informed support selection continues to improve performance after each method is given its own tuned learning rate. At the 12M-parameter tier, GradSVD lowers NLL by about 1.0% compared with the best principal-support variant and by about 1.4% compared with the best parameter-matched LoRA baseline. The gain becomes larger at the 6M-parameter tier, where GradSVD improves over LoRA by about 1.9%. This trend supports our main claim that loss-informed supports become more valuable under tighter adaptation budgets. SkewGrad is competitive at lower learning rates but becomes less stable as the learning rate increases; therefore, for stability, we use GradSVD as the default gradient-informed support in this low-resource language setting.

H.2 SkewGrad on MRPC and RTE

We provide two additional robustness analyses on MRPC and RTE to stress-test the loss-informed support-selection claim beyond the main six-task GLUE table. These two tasks are useful probes because they are relatively small, seed-sensitive sentence-pair classification tasks, so improvements on them are less likely to be explained solely by large-data averaging effects. In all experiments below, the support is constructed using the SkewGrad rule and the resulting support is fixed during training; we then compare the default orthogonal transform, the unconstrained free transform within the same support, and PSOFT under the corresponding setting.

The first analysis is a low-resource data-fraction sweep at fixed rank $r = 46$, where we vary the amount of training data while keeping the adaptation budget fixed. This tests whether SkewGrad remains useful when the calibration and downstream training signal are estimated from reduced supervision. The second analysis is a full-data rank sweep over $r \in \{16, 46, 64\}$, where we vary the adaptation budget while keeping the full training set available. This tests whether the observed gains depend on the main rank $r = 46$, or whether they persist across a broader parameter range. Unless otherwise stated, each setting uses the task-specific learning rate selected for that setting, and all reported values are averaged over five random seeds.

These experiments should be interpreted as robustness checks for the support-selection mechanism rather than as additional tests of the principal-support regime. In particular, the comparisons isolate whether the loss-informed SkewGrad support remains competitive against PSOFT when supervision is reduced or rank is changed, and whether the orthogonal/free distinction within the same support changes the outcome.

Table 24: Low-resource data-fraction sweep on MRPC and RTE for SkewGrad-support variants at fixed rank $r = 46$. All values are mean \pm standard deviation over five random seeds. $\text{LOFT}^{P_{\text{skew}}}$ uses the default orthogonal transform $T_r = T_{\text{orth}}$; $\text{LOFT}^{P_{\text{skew}}, T_{\text{free}}}$ uses the unconstrained free transform.

Task	Fraction	$\text{LOFT}_{r=46}^{P_{\text{skew}}}$	$\text{LOFT}_{r=46}^{P_{\text{skew}}, T_{\text{free}}}$	$\text{PSOFT}_{r=46}$
MRPC	10%	0.8394 \pm 0.0264	0.8502 \pm 0.0144	0.8171 \pm 0.0199
MRPC	20%	0.8640 \pm 0.0107	0.8636 \pm 0.0159	0.8487 \pm 0.0102
MRPC	40%	0.8952 \pm 0.0201	0.8840 \pm 0.0104	0.8692 \pm 0.0087
MRPC	60%	0.8988 \pm 0.0068	0.8984 \pm 0.0164	0.8751 \pm 0.0085
MRPC	80%	0.9080 \pm 0.0085	0.9017 \pm 0.0073	0.8982 \pm 0.0129
MRPC	100%	0.9216 \pm 0.0101	0.9265 \pm 0.0065	0.9086 \pm 0.0176
RTE	10%	0.6619 \pm 0.0426	0.6691 \pm 0.0326	0.6705 \pm 0.0405
RTE	20%	0.7252 \pm 0.0186	0.7381 \pm 0.0242	0.7262 \pm 0.0271
RTE	40%	0.8086 \pm 0.0320	0.8072 \pm 0.0276	0.7897 \pm 0.0078
RTE	60%	0.8158 \pm 0.0187	0.8388 \pm 0.0064	0.8115 \pm 0.0372
RTE	80%	0.8302 \pm 0.0195	0.8273 \pm 0.0176	0.8285 \pm 0.0168
RTE	100%	0.8683 \pm 0.0195	0.8677 \pm 0.0283	0.8675 \pm 0.0236

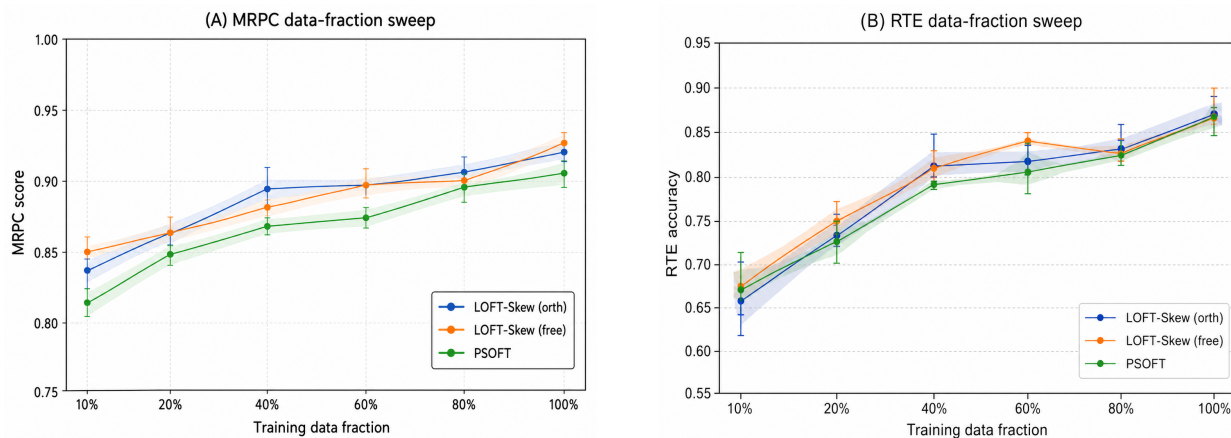


Figure 6: **Low-resource data-fraction robustness.** Panels (A) and (B) visualize the MRPC and RTE data-fraction sweeps in Table 24. Curves show mean performance over five seeds, with uncertainty indicating across-seed standard deviation.

Table 24 and Figure 6 show that the benefits of the theory-guided SkewGrad support are not confined to the full-data setting. On MRPC, both SkewGrad-support LOFT variants outperform PSOFT across all data fractions, with especially clear margins in the intermediate 40–60% regime and at full data. On RTE, the very low-resource regime is less stable at 10–20%, but from 40% onward the SkewGrad variants are consistently competitive and often stronger than PSOFT. These results support the view that loss-informed support selection remains useful when supervision is reduced.

Table 25: Full-data rank sweep on MRPC and RTE for SkewGrad-support variants. All values are mean \pm standard deviation over five random seeds. The sweep tests whether SkewGrad’s gains depend on the main rank $r = 46$ or persist across a broader parameter budget.

Task	Rank r	LOFT $^{P_{\text{skew}}}$	LOFT $^{P_{\text{skew}}, T_{\text{free}}}$	PSOFT
MRPC	16	0.9048 \pm 0.0072	0.9189 \pm 0.0106	0.8756 \pm 0.0068
MRPC	46	0.9216 \pm 0.0141	0.9265 \pm 0.0112	0.9086 \pm 0.0070
MRPC	64	0.9183 \pm 0.0087	0.9148 \pm 0.0103	0.9085 \pm 0.0068
RTE	16	0.7986 \pm 0.0337	0.8259 \pm 0.0298	0.7330 \pm 0.1507
RTE	46	0.8683 \pm 0.0283	0.8677 \pm 0.0456	0.8674 \pm 0.0147
RTE	64	0.8660 \pm 0.0316	0.8631 \pm 0.0186	0.8414 \pm 0.0194

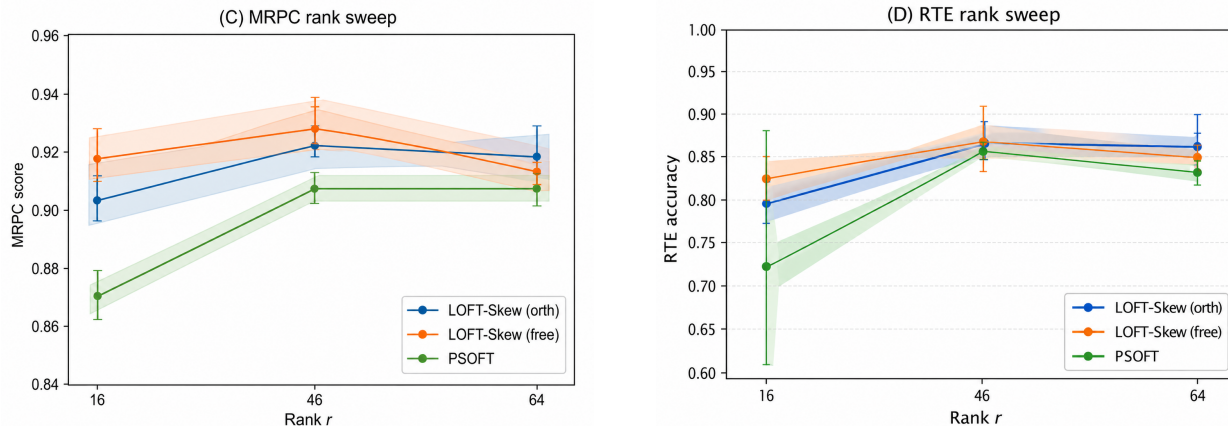


Figure 7: **Rank-sweep robustness.** Panels (C) and (D) visualize the MRPC and RTE rank sweeps in Table 25. Curves show mean performance over five seeds, with uncertainty indicating across-seed standard deviation.

Table 25 and Figure 7 show that the SkewGrad gains are not tied to a single narrowly tuned rank. On MRPC, both SkewGrad-support LOFT variants outperform PSOFT at all three ranks, with the strongest results around the main rank $r = 46$. On RTE, SkewGrad substantially improves over PSOFT at $r = 16$, remains competitive at $r = 46$, and stays clearly stronger at $r = 64$. Taken together, the data-fraction and rank sweeps indicate that the benefit of the theory-guided support persists across both supervision levels and parameter budgets, rather than arising only from one carefully chosen operating point.

I Additional Efficiency Measurements for Principal, GradSVD, and SkewGrad on GLUE

We further report supplementary wall-clock measurements on the six-task GLUE setup at rank $r = 46$. The goal is to quantify the training-time and parameter-cost profile of three support families under the same task-specific training protocol: principal support $P_r = P_{\text{prin}}$, GradSVD support $P_r = P_{\text{grad}}$, and SkewGrad support $P_r = P_{\text{skew}}$. For principal support, we additionally compare against PSOFT at the same rank. For GradSVD and SkewGrad, the reported wall-clock runtime includes the one-off calibration stage used to construct the fixed support before training the PEFT patch.

Because the support only changes the fixed basis P_r , the trainable parameter count is unchanged across support families for a fixed transform class and rank. Accordingly, all orthogonal LOFT variants at rank $r = 46$ use 74,520 non-classifier trainable parameters, while all free-transform LOFT

variants at the same rank use 152,352 non-classifier trainable parameters. PSOFT at rank $r = 46$ uses 81,144 non-classifier trainable parameters.

Table 26: End-to-end wall-clock training runtime in seconds on the six-task GLUE setup at rank $r = 46$. All runs use the same task-specific training protocol and the same NVIDIA V100 64GB GPU setting as Table 2. Runtime is measured from single-seed runs with seed 42 and rounded to the nearest second. #Params reports non-classifier trainable parameters. For GradSVD and SkewGrad supports, runtime includes the one-off calibration pass used to construct the support. For LOFT, $T_r = T_{\text{orth}}$ is used by default unless $T_r = T_{\text{free}}$ is shown.

Method / support	Transform	#Params	CoLA	MRPC	QNLI	RTE	SST-2	STS-B	Avg.
PSOFT $_{r=46}$	Ortho	81,144	3242	5793	29694	3927	15609	2879	10191
LOFT $_{r=46}^{P_{\text{prin}}}$	T_{orth}	74,520	2824	5479	28726	3926	13660	2556	9528
LOFT $_{r=46}^{P_{\text{grad}}}$	T_{orth}	74,520	2811	5666	28274	3973	13933	2610	9544
LOFT $_{r=46}^{P_{\text{skew}}}$	T_{orth}	74,520	2819	5765	28305	3936	13954	2640	9570
LOFT $_{r=46}^{P_{\text{prin}}}$	T_{free}	152,352	1395	4911	23161	3372	10295	1893	7504
LOFT $_{r=46}^{P_{\text{grad}}}$	T_{free}	152,352	1451	5176	26069	3574	10412	2030	8119
LOFT $_{r=46}^{P_{\text{skew}}}$	T_{free}	152,352	1483	5188	26074	3628	10321	1957	8108

Efficiency analysis. Table 26 highlights three points:

First, in the principal-support regime, orthogonal LOFT uses slightly fewer non-classifier trainable parameters than PSOFT at the same rank: 74,520 versus 81,144, an 8.2% reduction. It is also consistently faster than PSOFT in wall-clock time across the six GLUE tasks. This indicates that the additional PSOFT orthogonal transformation and magnitude factors introduce non-negligible per-step overhead, even though both methods operate at the same rank.

Second, $T_r = T_{\text{free}}$ uses more trainable parameters than $T_r = T_{\text{orth}}$, increasing the non-classifier LOFT parameter count from 74,520 to 152,352. Despite this larger parameter count, the free-transform variants are substantially faster than their orthogonal counterparts on all six tasks. This shows that runtime is not determined only by the number of trainable parameters; the cost of parameterizing the in-subspace orthogonal transform can dominate the small dense $r \times r$ update.

Third, gradient-informed support construction introduces little additional runtime relative to principal support. Among the orthogonal LOFT variants, GradSVD and SkewGrad require only 0.2% and 0.4% additional average runtime relative to principal support, respectively. GradSVD and SkewGrad also have nearly identical wall-clock runtime at matched transform type, showing that the extra cost of forming skew($W_0^\top G$) is negligible once calibration gradients have been collected. Even SkewGrad, the slowest orthogonal LOFT variant in average wall-clock time, remains 6.1% faster on average than PSOFT.